AFRL-RV-PS-
TR-2016-0120

PHYSICS AND APPLICATIONS OF UNIPOLAR BARRIERS IN INFRARED (IR) DETECTORS

Gary Wicks

University of Rochester
910 Genesee St., Ste 200
Rochester, NY 14611-3847

23 Aug 2016

Final Report

AIR FORCE RESEARCH LABORATORY
Space Vehicles Directorate
3550 Aberdeen Ave SE
AIR FORCE MATERIEL COMMAND
KIRTLAND AIR FORCE BASE, NM 87117-5776

DTIC COPY
NOTICE AND SIGNATURE PAGE

This report is the result of contracted fundamental research deemed exempt from public affairs security and policy review in accordance with SAF/AQR memorandum dated 10 Dec 08 and AFRL/CA policy clarification memorandum dated 16 Jan 09. This report is available to the general public, including foreign nationals. Copies may be obtained from the Defense Technical Information Center (DTIC) (http://www.dtic.mil).

AFRL-RV-PS-TR-2016-0120 HAS BEEN REVIEWED AND IS APPROVED FOR PUBLICATION IN ACCORDANCE WITH ASSIGNED DISTRIBUTION STATEMENT.

//SIGNED//
PAUL LEVAN
Program Manager

//SIGNED//
DAVID CARDIMONA
Technical Advisor, Space Based Advanced Sensing and Protection

//SIGNED//
JOHN BEAUCHEMIN
Chief Engineer, Spacecraft Technology Division
Space Vehicles Directorate

REPORT DOCUMENTATION PAGE

Form Approved
OMB No. 0704-0188

1. REPORT DATE *(DD-MM-YY)*	**2. REPORT TYPE**	**3. DATES COVERED** *(From - To)*
23-08-2016	Final Report	1 Oct 2014 – 29 Dec 2015

4. TITLE AND SUBTITLE
Physics and Applications of Unipolar Barriers in Infrared (IR) Detectors

5a. CONTRACT NUMBER
FA9453-14-1-0250

5b. GRANT NUMBER

5c. PROGRAM ELEMENT NUMBER
62601F

6. AUTHOR(S)
Gary Wicks

5d. PROJECT NUMBER
4846

5e. TASK NUMBER
PPM00015702

5f. WORK UNIT NUMBER
EF123915

7. PERFORMING ORGANIZATION NAME(S) AND ADDRESS(ES)
University of Rochester
910 Genesee St., Ste 200
Rochester, NY 14611-3847

8. PERFORMING ORGANIZATION REPORT NUMBER

9. SPONSORING / MONITORING AGENCY NAME(S) AND ADDRESS(ES)
Air Force Research Laboratory
Space Vehicles Directorate
3550 Aberdeen Ave., SE
Kirtland AFB, NM 87117-5776

10. SPONSOR/MONITOR'S ACRONYM(S)
AFRL/RVSW

11. SPONSOR/MONITOR'S REPORT NUMBER(S)
AFRL-RV-PS-TR-2016-0120

12. DISTRIBUTION / AVAILABILITY STATEMENT
Approved for public release; distribution is unlimited.

13. SUPPLEMENTARY NOTES

14. ABSTRACT
A recently invented, advanced, high performance infrared detector is the Unipolar Barrier detector. In this program, the effects of defects and surface currents on the performance of the detectors were investigated with modeling and experiment.

15. SUBJECT TERMS
barrier<or>barriers, detector<or>detectors, infrared<or>IR, unipolar

16. SECURITY CLASSIFICATION OF:			**17. LIMITATION OF ABSTRACT**	**18. NUMBER OF PAGES**	**19a. NAME OF RESPONSIBLE PERSON**
a. REPORT	**b. ABSTRACT**	**c. THIS PAGE**			David Cardimona
Unclassified	Unclassified	Unclassified	Unlimited	44	**19b. TELEPHONE NUMBER** *(include area code)*

Standard Form 298 (Rev. 8-98)
Prescribed by ANSI Std. 239.18

(This page intentionally left blank)

Table of Contents

List of Figures

Section **Page**

1.0 Summary

A recently invented, advanced, high performance infrared detector is the Unipolar Barrier detector. In this program, the effects of defects and surface currents on the performance of the detectors were investigated with modeling and experiment. In comparison to conventional pn-based infrared detectors, it was found that unipolar barrier detectors are dramatically less sensitive to performance degradation by defects. Surface conduction in infrared semiconducting materials was examined. The mechanisms of surface leakage in unipolar barrier detectors were investigated. A new implementation of unipolar barriers for infrared detection was demonstrated in a flat-band pn-based unipolar barrier detector.

2.0 Introduction

Modeling of dark currents in unipolar barrier detectors was performed. Verification of the modeling was obtained by constructing unipolar barrier detectors in III-V semiconductor structures grown by molecular beam epitaxy. Three main sub-topics were emphasized during this program: effects of defects on dark currents in infrared detectors, surface leakage current mechanisms in infrared detectors, and examination of a newly developed flat-band pn-based unipolar barrier detector.

3.0 Methods, Assumptions and Procedures

Effects of Defects on Dark Currents in infrared photodetectors

Two important cases where infrared photodetector performance may be dominated by defects in the semiconductor materials are: (1) construction of detectors of lattice-mismatched epitaxial material, and (2) operation of detectors in high radiation environments. In such cases, it was found than unipolar (nBn)detectors exhibit orders of magnitude less dark current that do conventional pn-based detectors, as shown in figure 1.

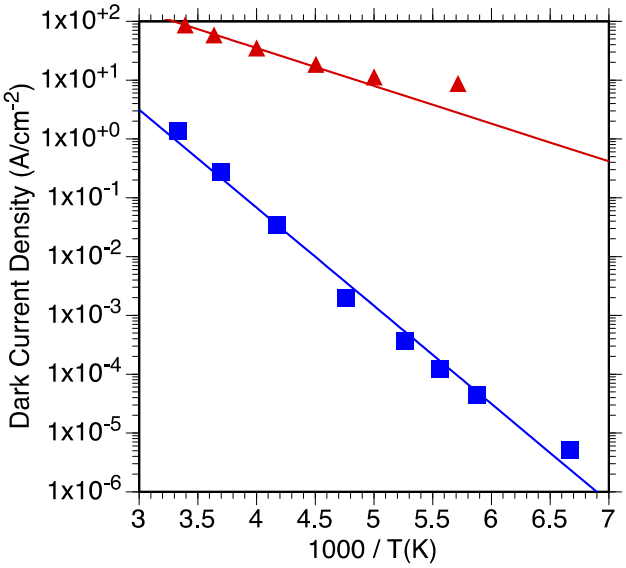

Figure 1. Arrhenius analysis for an InAs nBn detector (blue) and a conventional photodiode (red) grown on GaAs substrates. Even under elevated defect concentrations the nBn exhibits reduced dark current densities and full bandgap activation energies whereas the photodiode exhibits a reduced activation energy.

4.0 Results and Discussions

The observed reduction in dark current in defect-dominated unipolar (nBn) detector in comparison to conventional pn photodiodes was determined to be caused by the different current mechanisms of the two detectors: unipolar barrier dark current was found to be diffusion current whereas pn dark current was found to be generation-recombination current.

5.0 Conclusions

Surface Conduction Study of III-V Infrared Materials

Two materials that are important building blocks of III-V infrared detectors are InAs and GaSb. The electrical conductivity of the surfaces of these materials is important for understanding and controlling surface leakage currents of III-V infrared detectors. The electrical conductivity of these materials' surfaces was examined by measuring the temperature dependence of zero voltage conductance in pn junctions

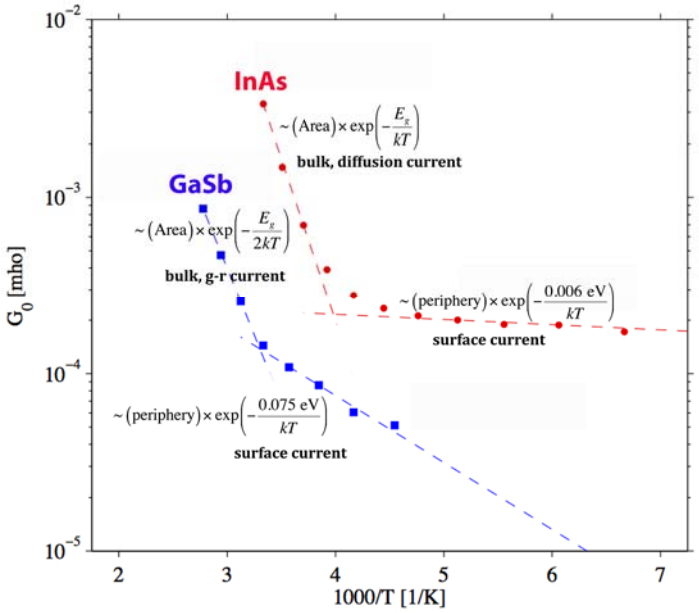

Fig. 2. Arrhenius graph of zero-voltage conductance for 210μm square InAs and GaSb pn junction devices. At higher temperatures, the conductance is dominated by bulk currents, whereas surface currents dominate at lower currents.

constructed of InAs and of GaSb. As shown in figure 2, at temperatures near room temperature, the conductances of the pn junctions scale with the cross sectional area of the devices, and hence is ascribed to bulk currents. However, upon cooling, the conductances are found to scaled with device periphery and thus are due to surface currents. The surface currents of InAs are found to be nearly independent of temperature, thus indicating a degenerate surface. The surface currents of GaSb are found to have a thermal activation energy of 75 meV, thus indicating a non-degenerate surface.

Appendix A

Infrared Physics & Technology 70 (2015) 111–114

Contents lists available at ScienceDirect

Infrared Physics & Technology

journal homepage: www.elsevier.com/locate/infrared

Flat-band pn-based unipolar barrier photodetector

D.E. Sidor *, G.R. Savich, X. Du, G.W. Wicks

The Institute of Optics, University of Rochester, Rochester, NY 14627, USA

ARTICLE INFO

Article history:
Received 11 August 2014
Available online 13 October 2014

Keywords:
Unipolar barrier
Infrared detector
Infrared photodetector
Dark current
Band edge engineering

ABSTRACT

This work presents a pn-based unipolar barrier detector architecture that exhibits no band bending under zero bias. A zero-bias flat band structure is created by utilizing materials with pre-aligned Fermi levels, which prevents charge transfer across the junction and depletion layer formation. The ideal structure shows no detectable g–r, tunneling, or surface leakage currents, and is more tolerant to variations in layer composition than other barrier detector architectures.

1. Introduction

The last decade has seen the emergence of the unipolar barrier device architecture as an attractive solution for achieving high performance infrared photodetectors. An "ideal" barrier architecture detector must possess several defining characteristics: it blocks majority carrier, surface, and tunneling leakage currents; allows for unimpeded flow of minority carriers; and suppresses generation–recombination (g–r) current by avoiding depletion regions. The nBn was the first (and remains the simplest) such detector, notable for its flat band structure under zero bias, and for its greatly improved dark current characteristics compared to conventional pn photodiodes [1].

Eliminating the depletion region from a pn-based structure is a significant challenge, yet one which must be met in order to realize a similarly "ideal" design. n- and p-type materials often have Fermi levels at different absolute energies, and devices formed from such materials will therefore incorporate some degree of band bending. The resulting depletion region g–r current may degrade their performance, making these devices less than ideal. The present work addresses this dilemma by demonstrating an ideal pn-based structure where the n- and p-type materials are carefully chosen to have pre-aligned Fermi levels, so that the device structure formed by joining these materials maintains flat energy bands throughout, and thus is free of zero-bias depletion regions.

2. Background

The depletion layer and band bending in a traditional pn junction result from charge transfer across the junction, which is needed to equalize the Fermi level throughout the device structure. This equalization process must occur in order to establish thermal equilibrium between the n- and p-type materials when the absolute energies of the Fermi levels in the unjoined materials are unequal. Note that this is always the case in a pn homojunction, where the Fermi level position depends on doping. It is frequently, but not always, the case in a pn heterojunction, where material choice also plays a role. This is not an issue in an nBn, because the n-type absorber and n-type collector materials have nearly (if not perfectly) aligned Fermi levels; in either case, any substantial band bending that would tend to move the Fermi level close to the middle of the bandgap is avoided. The resulting absence of associated depletion region g–r in this flat-band structure has been well-documented [2].

3. Device architecture

The goal of the present work is to apply design principles from the ideal nBn to create a similarly ideal, flat-band pn-based structure. In general, if the n-type collector of an nBn were replaced with an arbitrary p-type collector material, one of three possible situations must be the result. These situations are illustrated in Fig. 1.

(a) The Fermi level in the isolated p-type collector material is lower than the Fermi level in the isolated n-type absorber material. The joined structure will exhibit upward band

* Corresponding author.
E-mail address: sidor@optics.rochester.edu (D.E. Sidor).

http://dx.doi.org/10.1016/j.infrared.2014.09.037
1350-4495/

bending at the junction and downward band bending at the contact. The upward band bending at the junction creates a depletion region in the absorber, and the downward band bending at the contact creates a valence band barrier. The structure is identified by g–r current and increased thermal activation energy under reverse bias, and reduced thermal activation energy under forward bias.

(b) The Fermi level in the isolated p-type collector material is equal to the Fermi level in the isolated n-type absorber material. The joined structure will exhibit no band bending (under zero bias). The structure is identified by ideal, Auger-1-limited dark current, and full-bandgap thermal activation energy under both reverse and forward bias.

(c) The Fermi level in the isolated p-type collector material is higher than the Fermi level in the isolated n-type absorber material. The joined structure will exhibit downward band bending at the junction and upward band bending at the contact. The downward band bending at the junction creates a valence band barrier, and the upward band bending at the contact creates an accumulation layer. The structure is identified by increased thermal activation energy under both reverse and forward bias.

After selecting a specific material system in which to pursue this general design, some difficulty is encountered due to a lack of suitably precise information on absolute band energies. Some references exist [3], but the typical uncertainty of approximately 100 meV is too coarse for this purpose. Therefore a reasonable approach, and the one taken here, is to vary the composition of the p-type collector material among several different growths. The p-type collector material which results in the ideal band alignment can then be inferred by comparing these growths on the basis of their distinguishing performance characteristics described above.

4. Growth and fabrication

This work was performed with InAs-based materials. High-quality InAs substrates are readily available and $AlAs_{0.18}Sb_{0.82}$ is known to be an effective conduction band barrier with zero valence band offset [2]. GaSb-based materials were chosen for the p-type collector materials because the valence band of GaSb nearly aligns with the conduction band of InAs. Therefore, unintentionally-doped n-type InAs ($n \approx 10^{16}\,cm^{-3}$) and p-type GaSb ($p \approx 10^{17}\,cm^{-3}$) nearly possess the pre-aligned Fermi levels required to produce flat energy bands throughout the joined device structure.

One growth was performed with $GaAs_{0.09}Sb_{0.91}$ as the p-type collector material, which lattice-matches the InAs substrate. Exchanging gallium for aluminum has a small effect on lattice constant while increasing the bandgap of the collector layer, so it is a convenient method for varying between the possible band alignments outlined in Fig. 1. A second growth was performed with $Al_{0.12}Ga_{0.88}As_{0.09}Sb_{0.91}$ with the intent that the two growths would represent two of the three possible scenarios in Fig. 1, and one growth would represent the ideal scenario shown in Fig. 1(b).

Growths were performed by solid source molecular beam epitaxy on a Riber 32P reactor. After thermal desorption of the native oxide layer from the InAs substrate, absorber layer growth was initiated 75 °C above the InAs (001) [$(2 \times 4) \rightarrow (4 \times 2)$] transition temperature. Substrate temperature was not varied between layers, and only minimal growth stops were used (never exceeding 90 s) with the intent of preserving crystalline material quality at the interfaces.

Growths were processed into individual square mesas of varying sizes by contact photolithography and wet chemical etching. Ti/Au contacts were formed by electron beam evaporation and liftoff.

5. Device performance

The two epitaxially-grown structures were compared on the bases of dark current *J–V* characteristics, dark current thermal activation energy, and photoresponse. Each individual comparison provides partial information on the relative band alignments of the two epitaxial structures. Upon consideration of all three means for comparison, it becomes evident that the ternary collector structure possesses the ideal, flat band alignment shown in Fig. 1(b). The quaternary collector structure possesses band bending of the type shown in Fig. 1(a).

	Band Alignments in Isolated Materials	Band Diagrams of Joined Structures	Distinguishing Characteristics
(a)	$E_{F,p} < E_{F,n}$	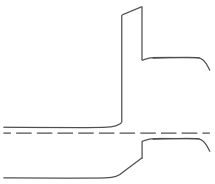	• Depletion layer in absorber • Hole barrier at contact • Lowest valence band offset
(b)	$E_{F,p} = E_{F,n}$	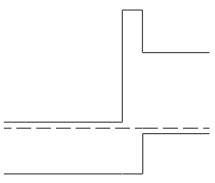	• No depletion or accumulation layers • No barriers for holes • Valence band offset ≈ bandgap of absorber
(c)	$E_{F,p} > E_{F,n}$	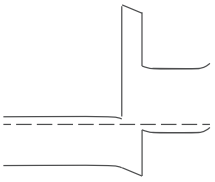	• Accumulation layer in absorber • Hole barrier at electron barrier • Highest valence band offset

Fig. 1. Possible zero-bias pn-based band structures and their distinguishing characteristics. $E_{F,p}$ refers to the absolute energy of the Fermi level in the isolated, bulk p-type material, and $E_{F,n}$ refers to the absolute energy of the Fermi level in the isolated, bulk n-type material.

5.1. Dark current characteristics

Dark current densities for the two device structures are shown at several different temperatures in Fig. 2. Both structures are rectifying, however the quaternary collector structure exhibits a significant rise in dark current density under reverse bias compared to the ternary collector structure. The source of this additional dark current mechanism in the quaternary collector structure is readily identified by referring to the band diagram in Fig. 1(a): it is g–r current resulting from the formation of a depletion region in the n-type absorber layer near the junction. The absence of this current mechanism in the ternary collector structure indicates that it possesses no such depletion region.

5.2. Thermal activation energy

Fig. 3 shows Arrhenius plots of dark current densities of the two device structures under 0.5 V reverse bias, and compares them to Rule 07. Rule 07 empirically describes the performance of state-of-the-art HgCdTe pn photodiodes [4]. Dark current density comparable to Rule 07 indicates that a device has reached the Auger-1 limit, thus making it a useful benchmark. Both device structures exhibit dark current densities that are within an order of magnitude of Rule 07.

The thermal activation energy of the dark current in the ternary collector structure under moderate reverse bias is approximately equal to the bandgap of the InAs absorber. This indicates that the dominant current mechanism is diffusion of holes that are thermally generated in the absorber layer, and that there are no additional valence band barriers to impede hole flow, consistent with the band diagram in Fig. 1(b). However the quaternary collector structure exhibits additional thermal activation energy in excess of the bandgap of the absorber. This can again be understood by referring to the band diagram in Fig. 1(a). In this structure, after thermal generation across the bandgap of the absorber, holes must also be thermally excited over the barrier that forms at the metal contact. The height of this barrier under moderate reverse bias is approximately 80 meV.

Fig. 4 shows the thermal activation energies of the two device structures as functions of applied bias. As previously stated, the thermal activation energy of the quaternary collector structure under moderate reverse bias is greater than that of the ternary collector structure, by about 80 meV, due to the presence of an additional valence band barrier. In contrast, the thermal activation energy of the quaternary collector structure under moderate forward bias is about 80 meV less than that of the ternary collector structure. The thermal activation energy in forward bias is the energy required to excite over the valence band offset; the reduction in forward-bias thermal activation energy of the quaternary collector structure is also consistent with the reduced valence band offset shown in Fig. 1(a).

The magnitudes of the thermal activation energy increase in reverse bias and decrease in forward bias, i.e. the contact barrier height and valence band offset reduction, are equal because they are results of the same effect: mis-alignment of the Fermi levels between isolated absorber and collector materials. The symmetry

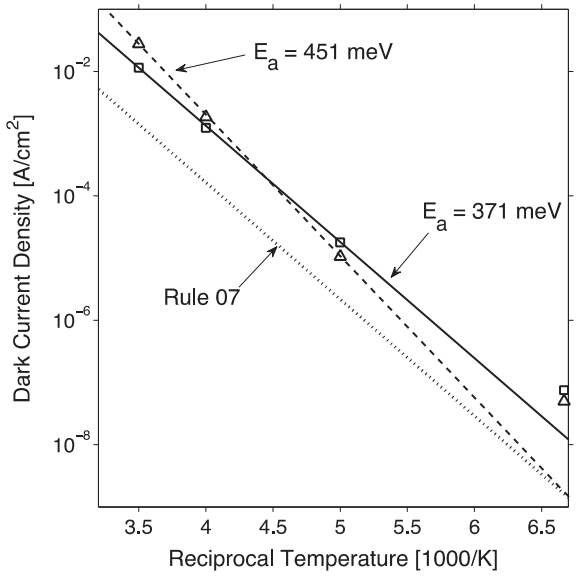

Fig. 3. Arrhenius plot of ternary collector structure (solid line with square markers) and quaternary collector structure (dashed line with triangle markers). Rule 07 is shown for 3.4 μm cutoff wavelength (dotted line).

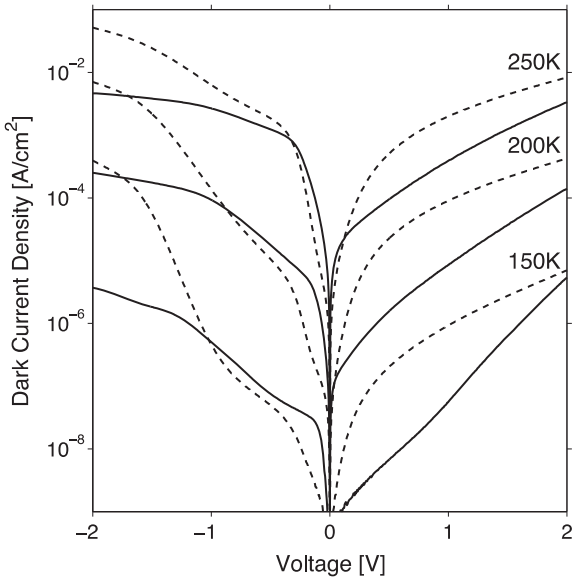

Fig. 2. Dark current densities of ternary collector structure (solid lines) and quaternary collector structure (dashed lines).

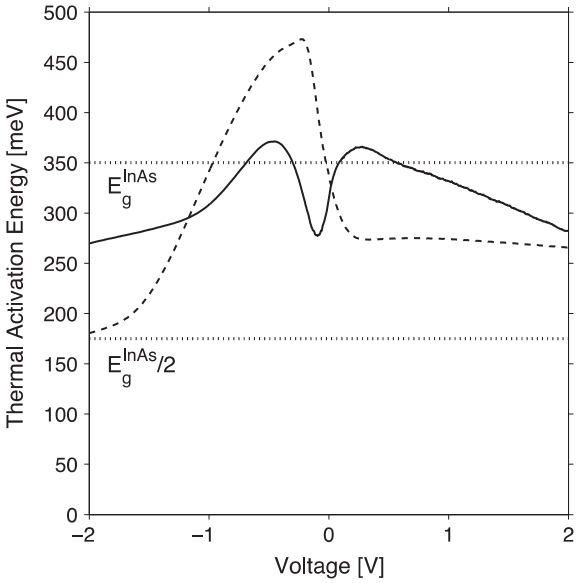

Fig. 4. Thermal activation energy of ternary collector structure (solid lines) and quaternary collector structure (dashed lines).

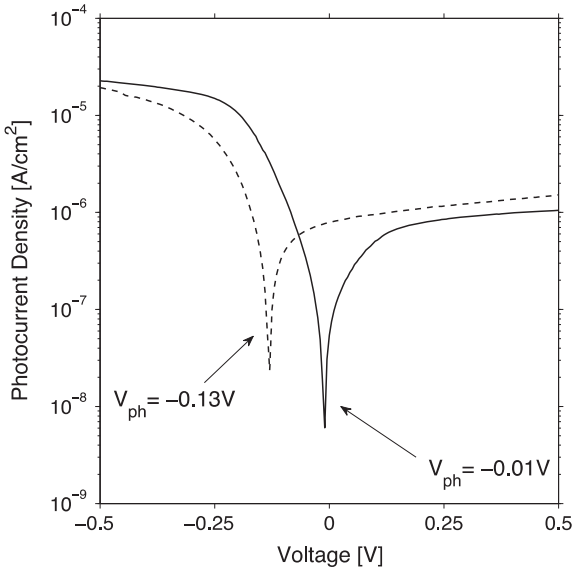

Fig. 5. Photoresponse of ternary collector structure (solid lines) and quaternary collector structure (dashed lines).

in thermal activation energy of the ternary collector structure with respect to voltage indicates that the absorber bandgap and valence band offset are equal in that structure, consistent with the band diagram in Fig. 1(b).

The thermal activation energy of the quaternary collector structure approaches half of the bandgap of the InAs absorber as the reverse bias is increased, signifying the onset of depletion region g–r current as stated in Section 5.1.

5.3. Photocurrent characteristics

Fig. 5 shows photocurrent densities for the two device structures measured at 150 K. The ternary collector structure shows essentially zero photovoltage, which is the expected result for a flat-band structure, since a built-in electric field is required to remove photogenerated carriers when no external bias is applied. The quaternary collector structure shows a non-zero photovoltage, which implies the existence of a built-in field and associated band bending (Fig. 1(a)).

To summarize the above comparisons, the ternary collector structure exhibits diffusion-limited dark current, a thermal activation energy equal to the bandgap of the absorber material, and essentially zero photovoltage. All three observations are consistent with the ideal, flat band diagram of Fig. 1(b). The quaternary collector structure, in contrast, shows an additional g–r dark current component indicating the existence of a depletion region in the absorber layer, increased thermal activation energy in reverse bias indicating the presence of a hole barrier, decreased thermal activation energy in forward bias indicating a reduced valence band offset, and a non-zero photovoltage indicating the presence of a built-in electric field, all of which is consistent with band bending of the type shown in Fig. 1(a).

6. Potential applications

There are two notable advantages to the ideal, flat band InAs/AlAsSb/GaAsSb photodetector. First, it offers a high-performance MWIR photodetector with a transparent collector layer, useful for any application in which top-side illumination is required. Second, the device architecture is more tolerant to variations in layer composition than other unipolar barrier designs. This is particularly true of the large-bandgap barrier layer where, in an nBn for example, any drift in the composition of the conduction band barrier layer will also result in the formation of a detrimental valence band barrier.

7. Conclusions

An ideal pn-based unipolar barrier photodetector may be formed in the InAs material system by replacing the n-type InAs collector layer of an InAs/$AlAs_{0.18}Sb_{0.82}$/InAs nBn with unintentionally-doped p-type $GaAs_{0.09}Sb_{0.91}$. This ternary material lattice-matches the InAs absorber and $AlAs_{0.18}Sb_{0.82}$ barrier layers, and its Fermi level is at the same absolute energy as the Fermi level in InAs. The structure formed by joining these materials has flat energy bands throughout, and its performance is comparable to an nBn and to other advanced barrier architecture detectors: its dark current density is within an order of magnitude of Rule 07; it has a thermal activation energy equal to the bandgap of the absorber material; and it shows no g–r, tunneling, or surface leakage currents. This high-performance MWIR photodetector incorporates a transparent collector layer, useful for applications requiring top-side illumination, and its overall performance is less sensitive to variations in layer composition than other advanced barrier architecture detector designs.

Conflict of interest

There is no conflict of interest.

Acknowledgements

This work was supported by the U.S. Army Research Office (W. Clark).

References

[1] S. Maimon, G.W. Wicks, NBn detector, an infrared detector with reduced dark current and higher operating temperature, Appl. Phys. Lett. 89 (2006) 151109.
[2] G.R. Savich, J.R. Pedrazzani, D.E. Sidor, S. Maimon, G.W. Wicks, Dark current filtering in unipolar barrier infrared detectors, Appl. Phys. Lett. 99 (2011) 121112.
[3] S. Tiwari, D.J. Frank, Empirical fit to band discontinuities and barrier heights in III–V alloy systems, Appl. Phys. Lett. 60 (1992) 630.
[4] W.E. Tennant, "Rule 07" revisited: still a good heuristic predictor of p/n HgCdTe photodiode performance?, J Electron. Mater. 39 (2010) 1030.

Appendix B

Defect related dark currents in III-V MWIR nBn detectors

G. R. Savich[a], D. E. Sidor[a], X. Du[a], M. Jain[a], C. P. Morath[b], V. M. Cowan[b], J. K. Kim[c], J. F. Klem[c], D. Leonhardt[c], S. D. Hawkins[c], T. R. Fortune[c], A. Tauke-Pedretti[c], G. W. Wicks*[a]
[a]The Institute of Optics, University of Rochester, 275 Hutchison Rd, Rochester, NY 14627-0186, USA; [b]Air Force Research Laboratory, Space Vehicles Directorate, 3550 Aberdeen Ave SE, Kirtland AFB, NM, USA 87117; [c]Sandia National Laboratories, Albuquerque, NM, USA 87185

ABSTRACT

The effect of defects on the dark current characteristics of MWIR, III-V nBn detectors has been studied. Two different types of defects are compared, those produced by lattice mismatch and by proton irradiation. It is shown that the introduction of defects always elevates dark currents; however the effect on dark current is different for nBn detectors and conventional photodiodes. The dark currents of nBn detectors are found to be more tolerant of defects compared to pn-junction based devices. Defects more weakly increase dark currents, and cooling reduces the defect-produced dark currents more rapidly in nBn detectors than in conventional photodiodes.

Keywords: infrared detectors, MWIR, nBn, photodiode, defects, irradiation, lattice mismatch, dark current.

1. INTRODUCTION

1.1 Barrier Architecture Detectors

The recent introduction of barrier architecture detectors has created the potential for improved performance for MWIR detection, particularly in the III-V material family[1]. This new class of detector has already shown significant advantages over conventional device architectures, like the pn junction based photodiode, due to their ability to naturally suppress many dark current mechanisms. Barrier architecture detectors have successfully shown suppression of surface leakage currents, depletion layer generation-recombination currents, trap-assisted tunneling, and direct band-to-band tunneling currents[2,3]. Furthermore, these devices have shown performance near Rule 07, indicating nearly Auger limited performance comparable to state-of-the-art HgCdTe MWIR detectors[4].

1.2 Defect-Dominated Dark Currents

In some applications for MWIR detectors, detectors may become limited by defect-related dark currents. The addition of defect states to the crystal structure of semiconductor-based detectors tends to increase the dark current of these devices. Significantly increasing the defect concentration can cause a measurable reduction in device performance[5]. Examples of cases where defect processes may dominate the dark current include grown-in defects such as in superlattice-based detectors; growth on mismatched substrates; and cases where devices will be subjected to the effects of a radiation filled environment. In such cases, using the detector architecture that minimizes the effects of the induced defects is an important consideration. The present work demonstrates that barrier architecture detectors have significant advantages over conventional pn photodiodes in these cases.

*wicks@optics.rochester.edu; phone 1 585 275-4867; fax 1 585 244-4936

Infrared Technology and Applications XL, edited by Bjørn F. Andresen, Gabor F. Fulop, Charles M. Hanson, Paul R. Norton, Proc. of SPIE Vol. 9070, 907011 · © 2014 SPIE
CCC code: 0277-786X/14/$18 · doi: 10.1117/12.2050535

2. GENERATION – RECOMBINATION CURRENTS IN PHOTODETECTORS

2.1 Depletion Region Generation – Recombination Current

Shockley-Read-Hall (SRH) theory for generation and recombination in pn junction depletion regions describes the effect of defects on dark current density[6,7]. The theory predicts that the main effects of temperature and defect concentration are given by:

$$J_{Depletion} = Ce^{-E_g/2kT} N_{defect} \tag{1}$$

For depletion layer limited generation, SRH theory indicates a thermal activation energy of half the bandgap, and a direct proportionality between dark current density and defect density.

2.2 Neutral Region Generation – Recombination Current

Shockley's original theory also describes generation processes in neutral regions of semiconductors[6,7]. This process has a smaller magnitude effect than depletion region generation, and thus has traditionally been less important, at least in pn junctions. Defect-related generation in neutral regions has different dependences on defect density and temperature than generation in depletion regions. The main effects in the neutral region are given by:

$$J_{Neutral} = Ce^{-E_g/kT} \sqrt{N_{defect}} \tag{2}$$

In the neutral region case, the dark current density due to defects maintains a full bandgap thermal activation energy, and is proportional to the square root of the defect density. Although neutral region defects will increase the dark current density, the effect is smaller than that of depletion region defects.

2.3 Generation – Recombination Currents in nBn Photodetectors and Conventional Photodiodes

In conventional pn junction based photodiodes, generation in both the neutral region and the depletion region may occur; however, depletion region generation is usually dominant, thus defect-related dark currents in pn photodiodes are approximately equal to the dark current generated in the depletion region as indicated in equation 1. nBn detectors, ideally, do not have depletion regions. When nBn detectors are defect-dominated, only neutral region generation currents are possible, therefore, dark current density for defect-dominated nBn's follows equation 2.

The differing generation currents that dominate defect-limited pn junction photodiodes and nBn detectors results in two practical effects. Defect related dark currents in nBn detectors show a reduced dependence on the defect density when compared to photodiodes, and cooling is more efficient in reducing nBn's dark current due to the full bandgap activation energy.

3. PERFORMANCE OF InAs PHOTODIODES AND nBn DETECTORS

InAs pn junction photodiodes were grown via molecular beam epitaxy (MBE) on both lattice matched and lattice mismatched substrates. Lattice mismatched samples were grown on both InP and GaAs substrates. The InAs buffer thickness on mismatched substrates was varied. Other studies have shown that the defect concentration due to the lattice-mismatch scales inversely with the buffer layer thickness[8]. Dark current is plotted against the inverse of the buffer thickness in figure 1.

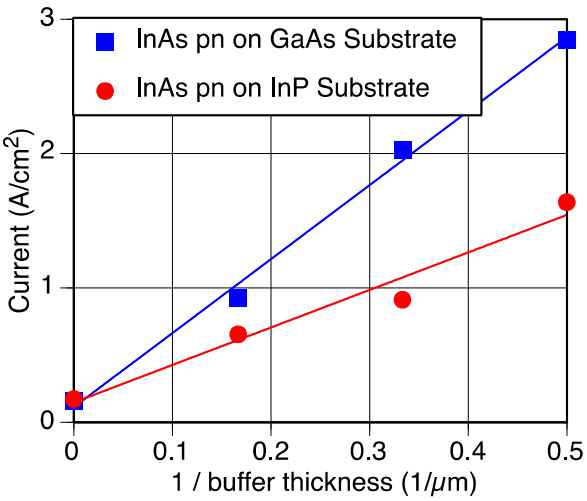

Figure 1. Current density vs. reciprocal buffer thickness for lattice mismatched InAs pn junction photodiodes on GaAs and InP substrates. Reciprocal buffer thickness is directly proportional to the density of defects that are associated with the lattice mismatch. Dark current density is shown to be well fit by a direct proportionality to the defect density.

The y-intercept point, indicated at zero reciprocal buffer thickness, or infinite buffer thickness, represent devices on lattice matched, InAs substrates. Since reciprocal buffer thickness is directly proportional to the defect density, fig. 1 shows that the dark current in mismatched pn photodiodes is directly proportional to the defect density, in agreement with equation 1. The lattice mismatch between InAs and GaAs is approximately twice that of the mismatch between InAs and InP, which causes the increased slope and thus elevated dark currents of the InAs photodiodes on GaAs substrates. The y-intercept value indicates the natural dark current present in the InAs detectors due to normal lattice-matched crystal growth and related dark current mechanisms. The horizontal axis indicates only the defects induced by the lattice mismatch.

Superlattice, MWIR nBn detectors were grown and irradiated with 63 MeV protons at low temperatures. The square of the dark current is plotted against proton fluence in figure 2.

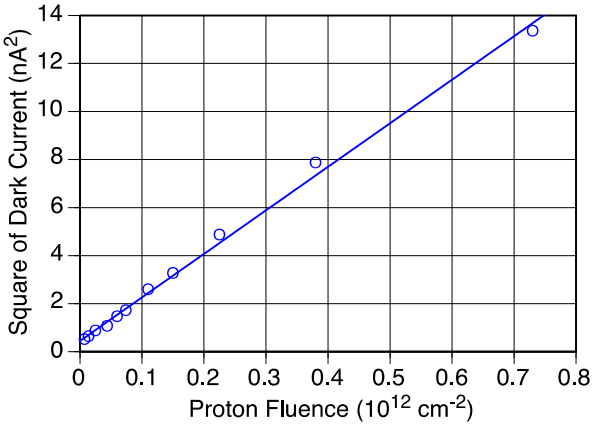

Figure 2. Square of the dark current as a function of proton fluence for proton irradiated MWIR nBn photodetectors. The square of the dark current is directly proportional to the proton fluence and the proton fluence is directly proportional to the defect density. The dark current in nBn detectors is proportional to the square root of the defect density.

There is a linear relationship between the square of the dark current and the proton fluence. Assuming that the density of irradiation-produced defects is proportional to the fluence, fig.2 indicates that the defect-related dark current in nBn detectors is proportional to the square root of the defect density, in agreement with equation 2. Since defect-related dark currents in conventional pn junction based photodiodes are directly proportional to the defect density, nBn detectors show an increased tolerance to defects by comparison. As in the case of the lattice-mismatched photodiodes, the y-intercept value is indicative of the natural dark current of the devices, present without the introduction of defects due to proton irradiation. The horizontal axis represents only the defects induced via proton irradiation at operating temperatures.

The temperature dependences of dark currents of both pn junction and nBn device architectures has also been studied. Figure 3 shows an Arrhenius graph of dark current density of conventional InAs photodiodes, grown both on a lattice matched, InAs substrate, and a lattice mismatched, GaAs substrate.

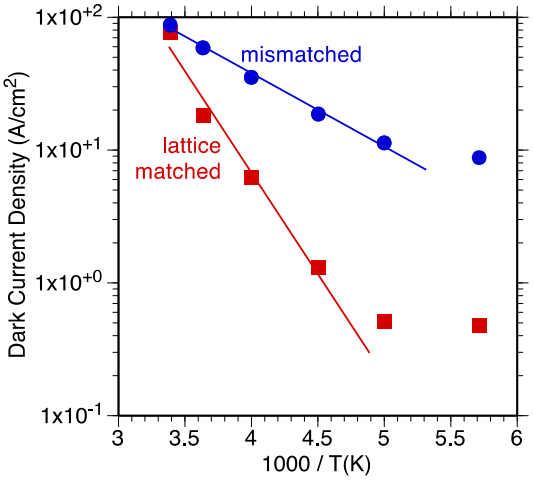

Figure 3. Dark current versus reciprocal temperature for lattice matched and lattice mismatched (GaAs substrate) InAs pn photodiodes. The thermal activation energy of lattice matched InAs photodiodes is equal to the bandgap of InAs (~0.31eV) down to ~210K at which point devices become surface leakage limited. Mismatched photodiodes on GaAs substrates exhibit activation energies slightly less than one half of the bandgap (~0.11eV) indicating behavior dominated by SRH generation in the depletion region.

Lattice matched, conventional InAs photodiodes show full bandgap activation energy, ~0.31 eV, from 300K to about 210K. Below this point, the dark current density becomes temperature independent, indicating the onset of surface leakage limited performance. The lattice mismatched InAs photodiode on a GaAs substrate shows an activation energy of ~0.11 eV, showing elevated dark currents on account of the increase in defects as well as a reduced rate of reduction in dark current density under cooling.

Dark current density as a function of temperature has also been studied for InAs nBn detectors on both InAs substrates and lattice mismatched GaAs substrates (figure 4).

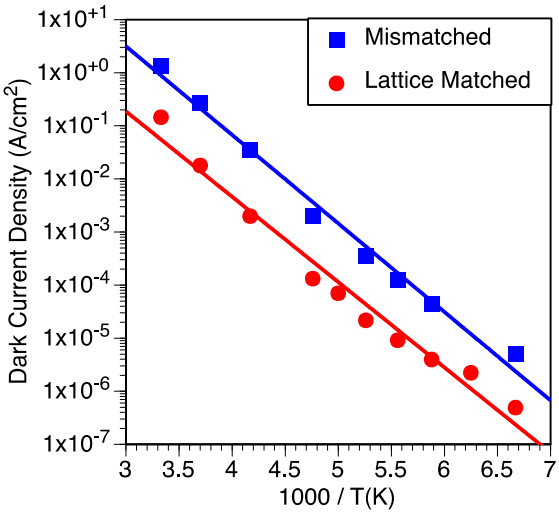

Figure 4. Dark current versus reciprocal temperature for lattice matched and lattice mismatched (GaAs substrate) InAs nBn detectors. The thermal activation energy (~0.35eV) is equal to the bandgap of InAs over the entire temperature range for both lattice matched and mismatched devices. Mismatched nBn detectors exhibit increased dark current densities compared to lattice matched nBn detectors.

The InAs nBn detectors on GaAs substrates show about an order of magnitude more dark current than comparable lattice matched InAs nBn's, indicating that inducing defects increases dark current levels in nBn detectors; however, the lattice mismatched nBn maintains a full bandgap activation energy, ~0.35 eV, equal to that of the lattice matched nBn across the entire measureable temperature range. This is a significant advantage that nBn detectors hold over conventional pn photodiodes. Although defect-limited nBn detectors and conventional photodiodes both show elevated dark currents compared to low defect concentration devices, the nBn maintains its full bandgap activation. This means defect-limited nBn detectors respond better to cooling than comparable pn junction based devices where depletion layer generation currents limit the defect-related activation energy to one half of the bandgap.

4. CONCLUSIONS

Defects elevate dark currents in both nBn detectors and conventional pn junction photodiodes; however, in cases where the defects limit dark currents, barrier architecture detectors offer significant benefits over pn photodiodes. nBn detectors are naturally more tolerant to increases in defect concentration, and defect-related dark currents reduce more quickly in nBn detectors under cooling. As a result, nBn detectors may be operated at a higher temperature than pn junction photodiodes in the presence of high defect levels. Defect-limited InAs nBn's show about four orders of magnitude less dark current, compared to conventional photodiodes at an operating temperature of 200K.

REFERENCES

[1] Maimon, S. and Wicks, G.W., "nBn detector, an infrared detector with reduced dark current and higher operating temperature," Appl. Phys. Lett. 89 (15), 151109 (2006).

[2] Pedrazzani, J.R., Maimon, S., and Wicks, G.S., "Use of nBn structures to suppress surface leakage currents in unpassivated InAs infrared photodetectors," Electron Lett. 44 (25), 1487 (2008).

[3] Savich, G.R., Pedrazzani, J.R., Sidor, D.E., Maimon, S., Wicks, G.W., "Dark current filtering in unipolar barrier infrared detectors," Appl. Phys. Lett. 99 (12), 121112 (2011).

[4] Tennant, W.E., Lee, D., Zandian, M., Piquette, E., and Carmody, M., "MBE HgCdTe Technology: A Very General Solution to IR Detection, Described by 'Rule 07', a Very Convenient Heuristic," Journal of Electronic Materials 37 (9), 1406 (2008).

[5] Cowan, V.M., Morath, C.P., Hubbs, J.E., Myers, S., Plis, E., Krishna, S., "Radiation tolerance characterization of dual band InAs/GaSb type-II strain-layer superlattice pBp detectors using 63 MeV protons," Appl. Phys. Lett. 101 (25), 251108 (2012).

[6] Shockley, W., Read, Jr., W.T., "Statistics of the recombinations of holes and electrons." Phys. Rev. 87 (5), 835 (1952).

[7] Sah, C.-T, Noyce, R.N., Shockley, W., "Carrier generation and recombination in p-n junctions and p-n junction characteristics," Proc. IRE 45 (9), 1228 (1957).

[8] Krier, A., Suleiman, W., "Uncooled photodetectors for the 3-5μm spectral range based on III-V heterojunctions," Appl. Phys. Lett. 89 (8), 083512 (2006).

Appendix C

Effect of defects on III-V MWIR nBn detector performance

G. R. Savich[a], D. E. Sidor[a], X. Du[a], C. P. Morath[b], V. M. Cowan[b], G. W. Wicks*[a]
[a]The Institute of Optics, University of Rochester, 275 Hutchison Rd, Rochester, NY 14627-0186, USA; [b]Air Force Research Laboratory, Space Vehicles Directorate, 3550 Aberdeen Ave SE, Kirtland AFB, NM, USA 87117

ABSTRACT

Under elevated defect concentrations, MWIR, III-V nBn detectors exhibit diffusion limited performance with elevated dark current densities. The resulting diffusion current is limited by the generation of carriers through defect states in the neutral n-type absorber and a dark current dependence on the defect density described by one of two limits, a short absorber or long absorber limit. This characteristic contrasts that exhibited by defect limited, conventional pn junction based photodiodes which exhibit performance limited by Shockley-Read-Hall generation in the depletion layer rather than diffusion based processes.

Keywords: infrared detectors, MWIR, nBn, photodiode, defects, irradiation, lattice mismatch, dark current.

1. INTRODUCTION

1.1 Barrier Architecture Detectors with Elevated Defect Concentrations

Barrier architecture detectors have shown considerable promise as an alternative to conventional structures for high performance infrared detection since the nBn was first introduced[1]. The ability of these detector structures to naturally suppress some dark current mechanisms, such as surface leakage current, generation-recombination current generated in depletion layers, and tunneling currents, is a significant advantage; however, performance matching or exceeding Rule 07 has not been achieved[2,3]. This suggests that barrier architecture detectors have not exhibited Auger limited performance [4].

One consideration that may contribute to this elevated dark current is a high defect concentration as the introduction of defects typically increases dark currents. There are several possible sources of defects in compound semiconductor-based detectors. In some cases, defects can be grown into the structure either as defects directly grown into the bulk crystal lattice, dislocations from growth on mismatched substrates, or layer interface defects in type-II strained layer superlattices. In some applications for MWIR detection, devices may operate in environments in which exposure to radiation is a concern. In this case, even a high performance detector may become severely defect limited as irradiation causes a significant reduction in performance[5]. As elevated dark currents will increase noise in the detector, it is important to understand the impact elevated defect concentrations will have on barrier architecture detector performance.

2. GENERATION – RECOMBINATION CURRENTS IN PHOTODETECTORS

The Shockley-Read-Hall (SRH) theory for generation-recombination in semiconductor structures provides a useful description of the effects defects have on dark currents generated in depletion regions and neutral regions of semiconductors[6,7]. Each of these regions exhibit a different current characteristic and varying dark current dependencies on the defect density.

*wicks@optics.rochester.edu; phone 1 585 275-4867; fax 1 585 244-4936

Nanophotonics and Macrophotonics for Space Environments VIII, edited by Edward W. Taylor, David A. Cardimona, Proc. of SPIE Vol. 9226, 92260R · © 2014 SPIE
CCC code: 0277-786X/14/$18 · doi: 10.1117/12.2064229

2.1 Depletion Region Generation – Recombination Current

Conventional pn-junction based photodiodes are typically limited by Shockley-Read-Hall (SRH) generation in the depletion region[6,7]. For this case, the theory predicts a thermal activation energy of half the bandgap and a dark current density that is directly proportional to the defect density:

$$J_{Depletion} = C_1 e^{-E_g/2kT} N_{defect} \tag{1}$$

The half-bandgap thermal activation energy is typically observed in detectors that are defect limited in a given temperature range[8].

2.2 Neutral Region Generation – Recombination Current

Generation-Recombination currents may manifest in neutral regions of semiconductors when there is an elevated defect concentration. This effect is also described in Shockley's original theory[6,7]. The magnitude of neutral region SRH current is typically significantly lower than depletion region SRH currents and, thus, this mechanism has typically been less important even though both mechanisms will exist in defect limited pn-junction based devices. With the emergence of barrier architecture detectors, which do not exhibit depletion region SRH currents under reasonable biases, this neutral region SRH effect has greater significance.

The dark current density for neutral region SRH generation can be obtained by combining Shockley's neutral region generation with the diffusion of carriers. Two limits result from the diffusion theory including a short absorber or long diffusion length and a long absorber or short diffusion length limit. Each case exhibits a different dependence on the defect concentration and corresponds to a different magnitude of defect concentration in the device.

The short absorber limit can also be described as a long diffusion length case. Here, the diffusion length is longer than the thickness of the absorber region. This is the optimum arrangement for high quantum efficiency infrared detectors as it guarantees that the highest percentage of photogenerated carriers are collected at the contacts before recombination can occur. The characteristics of the dark current density for this case are generally described by:

$$J^{Neutral}_{short,abs} = C_2 e^{-E_g/kT} N_{Defect} \tag{2}$$

In the short absorber limit for neutral region generation, the dark current density due to defects maintains a full bandgap thermal activation energy, and is directly proportional to the defect density.

The long absorber limit describes performance when the absorber thickness is greater than the diffusion length. The performance in this case varies slightly from the previous case, primarily when it comes to the dependence on defect density. The general dark current density characteristics for the long absorber or short diffusion length limit follow:

$$J^{Neutral}_{long,abs} = C_2 e^{-E_g/kT} \sqrt{N_{Defect}} \tag{3}$$

Like the short absorber limit, the thermal activation energy for the long absorber follows the full bandgap energy, but now, the dark current density is proportional to the square root of the defect density. This indicates that when a device enters

the long absorber limit, further increasing the defect concentration will have a smaller effect on the increasing dark current density when compared to a device operating in the short absorber limit.

2.3 Short and Long Absorber Limits in Practice

High performance MWIR detectors typically exhibit long diffusion lengths far in excess of the absorber thickness. These high quantum efficiency, non-defect limited detectors will operate in the short absorber limit. In this case, there will be some low level defect related dark current, but it will be small compared to the limiting current, typically Auger generation current and subsequent diffusion of carriers. This Auger limited performance has not yet been demonstrated in III-V barrier architecture detectors.

In nBn detectors with a moderate increase in defect concentration the limiting diffusion current may remain in the short absorber limit where the diffusion length is still long relative to the thickness of the absorber but the performance is now limited by defect induced neutral region SRH generation. To date, this is the best that has been achieved for barrier architecture detectors indicated by dark current densities above those predicted by Rule 07[3,4].

Detectors with very high defect concentrations may enter the short diffusion length regime or long absorber limit, where the diffusion length is now shorter than the thickness of the absorber. In this case, barrier architecture devices will be limited by neutral region SRH currents in accordance with long absorber limited diffusion. Even though this limit exhibits a reduced dependence of the dark current on increasing defect density, this limit suggests that significant damage has been done to the epitaxial structure and thus should be avoided if at all possible.

Ideally, it is best to operate a device in a low defect concentration state where the limiting current mechanism is not defect related. If defects cannot be avoided, it is better to minimize the accumulated defects and remain in the short absorber limit where degradation in performance is minimized.

3. DARK CURRENT DEPENDENCE ON DEFECT DENSITY

It has been shown that the defect concentration due to the lattice-mismatch scales inversely with the buffer layer thickness, thus InAs pn junction photodiodes were grown on both lattice matched and lattice mismatched substrates[9]. The photodiodes were grown via molecular beam epitaxy on InAs, InP, and GaAs substrates and the InAs buffer thicknesses were varied on the InP and GaAs substrate growths. Dark current characteristics were collected and dark current density was plotted against the inverse of the buffer thickness (figure 1).

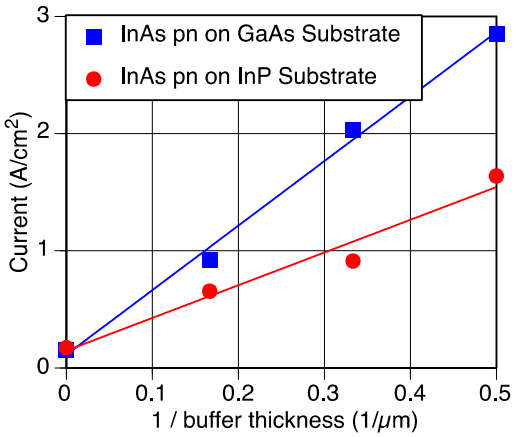

Figure 1. Current density vs. reciprocal buffer thickness for InAs pn junction photodiodes on mismatched substrates. The induced defect density shares a direct proportionality with the reciprocal of the buffer thickness and thus the dark current density scales directly with increasing defect concentration.

Lattice matched InAs photodiodes are indicated as points with zero reciprocal buffer thickness. The linear relationship between current density and reciprocal buffer thickness indicates a direct proportionality between dark current density and increases in defect concentration as predicted by the SRH theory for generation in depletion regions of pn-junction based devices.

Proton irradiated nBn detectors have been considered. In the case of barrier architecture detectors, the neutral region SRH and diffusion model predicts one of two behaviors manifest in two different dependences on the defect concentration. It is useful to consider the predicted behavior of dark current as a function of proton fluence (figure 2).

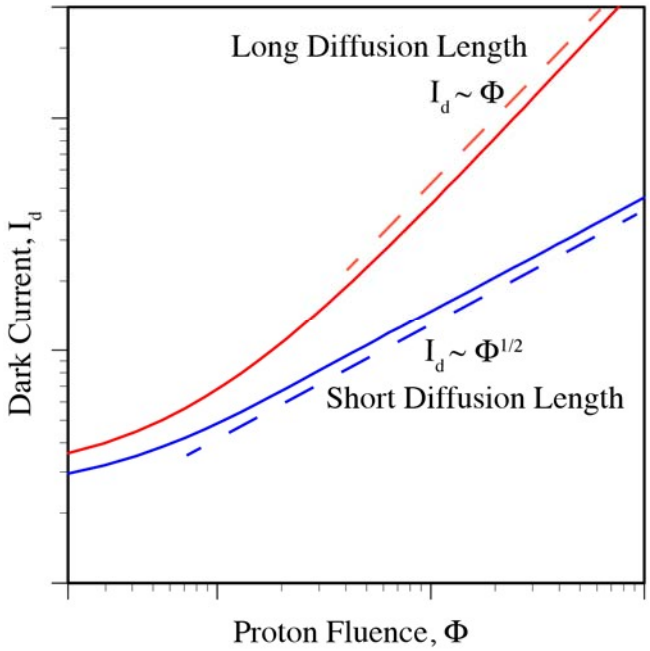

Figure 2. Predicted relationship between dark current and proton fluence for both the long diffusion length case or short absorber limit and the short diffusion length case or long absorber limit. In both cases, low fluence levels show dark currents limited by native defects in the epitaxial structure before radiation damage significantly increases the dark current. At higher fluence levels, dark current either scales directly with or with the square root of the proton fluence for the long and short diffusion length cases respectively.

Figure 2 shows predicted performance under increasing proton fluence for both the long diffusion length case, or short absorber limit, and the short diffusion length, or long absorber limit. In both cases, under low fluences the model predicts performance limited by native defects in the epitaxial structure. These defects are already inherent in the crystal structure before any irradiation occurs. Low fluence levels do not significantly increase the defect concentration and thus the dark current density. Under moderate to high proton fluences, the defect concentration increases enough to cause an increase in the dark current. It is assumed that defect concentration increases linearly with proton fluence. Here, the difference in proportionality between dark current and defect density in the two limits can be seen. The long diffusion length limit will show a direct proportionality between dark current and proton fluence while the short diffusion length limit shows that dark current is proportional to the square root of the proton fluence.

A superlattice, MWIR nBn detector was irradiated with 63 MeV protons at a low operating temperature[8]. The dark current is plotted against proton fluence in figure 3.

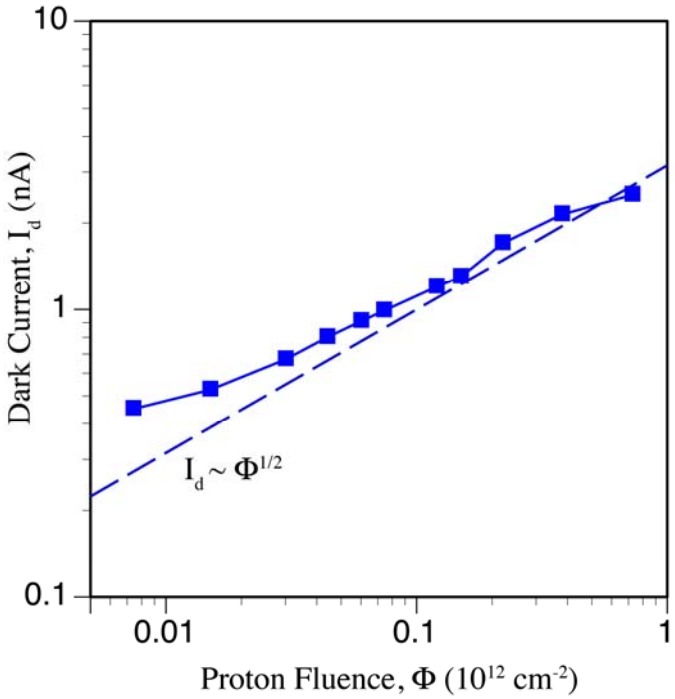

Figure 3. Dark current as a function of proton fluence for a proton irradiated MWIR nBn photodetector. Under low fluence levels, performance of the detector is primarily limited by native defects in the epitaxial structure. Higher fluence levels indicate dark current is proportional to the square root of the defect density indicating performance in the short diffusion length or long absorber limit.

Under low proton fluence levels, there is only a minimal increase in the dark current indicating that low proton fluences are not significantly increasing the defect concentration beyond the native defect concentration of the epitaxial structure in accordance with the model and figure 2. Moderate to high proton fluences, however, do result in a noticeable increase in dark current with increasing proton fluence. Under these conditions, the dark current increases with the square root of the proton fluence meaning the dark current is proportional to the square root of the defect density. This indicates that the device is operating in the short diffusion length regime where the absorber is thicker than the diffusion length. The native defects of this growth were high enough that this device was operating in the short diffusion length limit even before irradiation of the device. If the epitaxial growth of the device yielded a lower native defect concentration, it is likely the detector would have had a longer diffusion length and would have operated in the long diffusion length limit, even under moderate proton fluences.

4. CONCLUSIONS

The manner in which defects increase dark currents in photodetectors is dependent on both device architecture and defect concentrations. Conventional pn junction-based photodiodes under high defect levels follow the SRH model for generation in the depletion region of a pn junction while barrier architecture detectors, particularly the nBn, show defect limited performance in accordance with SRH generation in the neutral region followed by the diffusion of carriers. For the nBn, one of two cases may dominate. The long diffusion length limit where the absorber thickness is shorter than the diffusion length indicates low defect or moderate defect levels and defect related currents will scale directly with increases in defect density. For higher defect concentrations, the diffusion length becomes shorter than the absorber thickness indicating the short diffusion length limit. Here, the dark current scales as the square root of the defect density; however, this limit indicates significant damage to the semiconductor structure and thus reduced performance.

ACKNOWLEDGEMENT

The authors wish to acknowledge JK Kim, JF Klem, D Leonhardt, SD Hawkins, TR Fortune, and A Tauke-Pedretti of Sandia National Laboratories in Albuquerque, New Mexico for the design, growth, and fabrication of the MWIR nBn used for the irradiation study.

REFERENCES

[1] Maimon, S. and Wicks, G.W., "nBn detector, an infrared detector with reduced dark current and higher operating temperature," Appl. Phys. Lett. 89 (15), 151109 (2006).
[2] Pedrazzani, J.R., Maimon, S., and Wicks, G.W., "Use of nBn structures to suppress surface leakage currents in unpassivated InAs infrared photodetectors," Electron Lett. 44 (25), 1487 (2008).
[3] Savich, G.R., Pedrazzani, J.R., Sidor, D.E., Maimon, S., Wicks, G.W., "Dark current filtering in unipolar barrier infrared detectors," Appl. Phys. Lett. 99 (12), 121112 (2011).
[4] Tennant, W.E., Lee, D., Zandian, M., Piquette, E., and Carmody, M., "MBE HgCdTe Technology: A Very General Solution to IR Detection, Described by 'Rule 07', a Very Convenient Heuristic," Journal of Electronic Materials 37 (9), 1406 (2008).
[5] Cowan, V.M., Morath, C.P., Hubbs, J.E., Myers, S., Plis, E., Krishna, S., "Radiation tolerance characterization of dual band InAs/GaSb type-II strain-layer superlattice pBp detectors using 63 MeV protons," Appl. Phys. Lett. 101 (25), 251108 (2012).
[6] Shockley, W., Read, Jr., W.T., "Statistics of the recombinations of holes and electrons." Phys. Rev. 87 (5), 835 (1952).
[7] Sah, C.-T, Noyce, R.N., Shockley, W., "Carrier generation and recombination in p-n junctions and p-n junction characteristics," Proc. IRE 45 (9), 1228 (1957).
[8] GR Savich, DE Sidor, X Du, M Jain, CP Morath, VM Cowen, JK Kim, JF Klem, D Leonhardt, SD Hawkins, TR Fortune, A Tauke-Pedretti, GW Wicks, "Defect Related Dark Currents in III-V MWIR nBn Detectors," SPIE Defense+ Security, 907011-907011-6 (2014).
[9] Krier, A., Suleiman, W., "Uncooled photodetectors for the 3-5μm spectral range based on III-V heterojunctions," Appl. Phys. Lett. 89 (8), 083512 (2006).

AIP Applied Physics Letters

Diffusion current characteristics of defect-limited nBn mid-wave infrared detectors

G. R. Savich, D. E. Sidor, X. Du, C. P. Morath, V. M. Cowan, and G. W. Wicks

Citation: Applied Physics Letters **106**, 173505 (2015); doi: 10.1063/1.4919450
View online: http://dx.doi.org/10.1063/1.4919450
View Table of Contents: http://scitation.aip.org/content/aip/journal/apl/106/17?ver=pdfcov
Published by the AIP Publishing

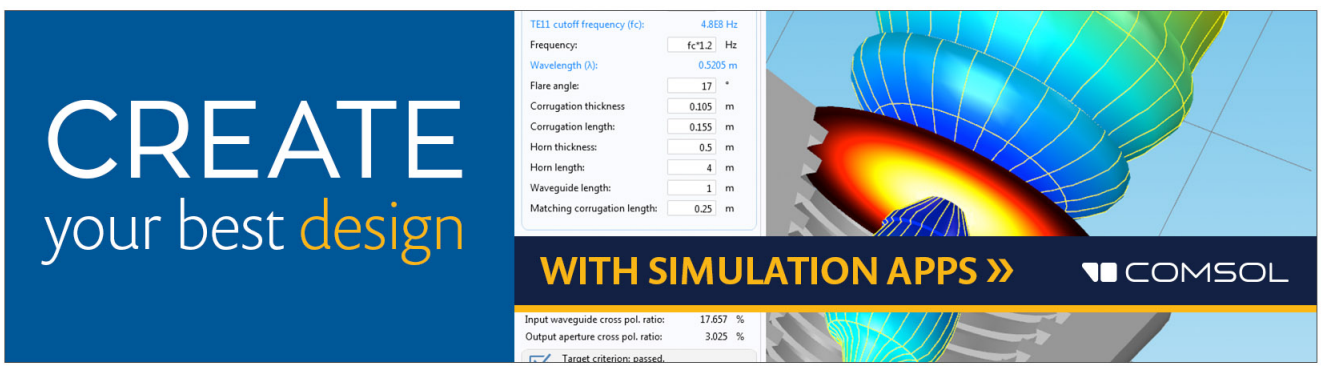

Diffusion current characteristics of defect-limited nBn mid-wave infrared detectors

G. R. Savich,[1] D. E. Sidor,[1] X. Du,[1] C. P. Morath,[2] V. M. Cowan,[2] and G. W. Wicks[1,a)]
[1]*The Institute of Optics, University of Rochester, 275 Hutchison Rd., Rochester, New York 14627-0186, USA*
[2]*Air Force Research Laboratory, Space Vehicles Directorate, 3550 Aberdeen Ave. SE, Kirtland AFB, New Mexico 87117, USA*

(Received 31 December 2014; accepted 20 April 2015; published online 28 April 2015)

Mid-wave infrared, nBn detectors remain limited by diffusion current generated in the absorber region even when defect concentrations are elevated. In contrast, defect-limited conventional pn-junction based photodiodes are subject to Shockley-Read-Hall generation in the depletion region and subsequent carrier drift. Ideal nBn-architecture devices would be limited by Auger 1 generation; however, typical nBn detectors exhibit defect-dominated performance associated with Shockley-Read-Hall generation in the quasi-neutral absorbing region. Reverse saturation current density characteristics for defect-limited devices depend on the minority carrier diffusion length, absorbing layer thickness, and the dominant minority carrier generation mechanism. Unlike pn-based photodiodes, changes in nBn dark current due to elevated defect concentrations do not manifest at small biases, thus, the zero bias resistance area product, R_oA, is not a useful parameter for characterizing nBn-architecture photodetector performance. © *2015 AIP Publishing LLC*.
[http://dx.doi.org/10.1063/1.4919450]

Infrared detectors with the nBn architecture or related unipolar barrier architectures perform differently under the presence of elevated defect concentrations when compared to conventional pn-junction based photodiodes.[1] Understanding this difference in performance is critical to understanding the performance of current state-of-the-art nBn detectors as well as the performance limitations of nBn detectors, in general. There are several cases where defect concentrations may become elevated in devices used for infrared detection. Detectors utilized for space-based applications or used in radiation-filled environments may initially exhibit low defect concentrations, but irradiation caused by the detector environment can increase defect concentrations significantly.[2] Additionally, absorbing layers grown as strained layer superlattices or materials lattice mismatched to the substrate can increase the density of defects dramatically.[1,3]

Under elevated defect concentrations, conventional pn junction-based devices usually become dominated by the well documented and understood effects of generation-recombination (g-r) or Shockley-Read-Hall (SRH) dark current generated in the depletion region of the pn junction. Carriers generated via depletion region SRH are subject primarily to carrier drift due to the build in electric field rather than diffusion of carriers. Such defect-limited pn junctions exhibit SRH dark current that decreases with temperature and shows an activation energy of one half of the bandgap energy, and increases in proportion to the defect density, as described by Shockley's theory. The reverse saturation current density for this mechanism is given by

$$J_{pn} = \frac{en_i(T)L_{dep}(V)}{2\tau_o}\frac{2kT}{e(V_{bi}-V)} \times \sinh\left(-\frac{eV}{2kT}\right)\int_0^\infty \frac{du}{u^2+2ue^{-\frac{eV}{2kT}}+1}, \quad (1)$$

where e is the charge of the electron, $L_{dep}(V)$ is the width of the depletion region, τ_o is the minority carrier lifetime due to the SRH process, k is the Boltzmann constant, T is the temperature, V_{bi} is the built-in voltage of the junction, and V is the applied voltage. At reverse voltages larger than a few kT, the dominant temperature-dependence in the above expression is contained in the n_i factor, where $n_i(T) \propto \exp(E_g/2kT)$ is the intrinsic carrier concentration.[4,5]

Ideal nBn detectors would be expected to exhibit diffusion limited performance originating from Auger 1 generation. Auger limited performance is associated with low defect concentrations, long diffusion lengths, and high quantum efficiency. These detectors should exhibit performance matching that suggested by Rule 07, a metric used to describe the performance of state-of-the-art HgCdTe infrared detectors, the best mid-wave infrared (MWIR) detectors currently available.[6] To date, however, barrier architecture detectors have not exhibited performance matching Rule 07, yet still show diffusion limited performance.[7] These diffusion currents originate from SRH, rather than Auger, processes. Furthermore, nBn detectors with defect concentrations elevated beyond the native defect concentration, in contrast to conventional photodiodes, also maintain diffusion-limited performance under moderate biases; however, the dark current density is elevated. For both of these cases, the diffusion current originates from a SRH process in the quasi-neutral absorber rather than Auger 1 generation.

Under the boundary condition requiring the current due to holes to be zero at the substrate interface of the nBn

a)wicks@optics.rochester.edu

0003-6951/2015/106(17)/173505/4/$30.00

absorber, it has been shown that the diffusion saturation current density for a quasi-neutral n-region can be described by

$$J_S = \frac{en_i^2 L_{diff}}{N_{donor}\tau}\tanh\left(\frac{L_{abs}}{L_{diff}}\right), \quad (2)$$

where L_{diff} is the minority carrier diffusion length, N_{donor} is the donor density, τ is the minority carrier lifetime, and L_{abs} is the thickness of the absorbing region.[8] The minority carrier lifetime is dependent on the dominant minority carrier generation mechanism in the absorber. For a defect limited nBn detector, the limiting lifetime is described by Shockley's theory. The original SRH theory applies to both the depletion layer in a pn junction and the quasi-neutral semiconductor region away from the junction. These neutral region SRH currents arise from defect states in the bandgap of the neutral region. The minority carrier lifetime for this generation mechanism can be described by

$$\tau_{SRH} = \frac{1}{v\sigma N_{defect}}, \quad (3)$$

where v is the electron velocity, σ is the defect capture cross section, and N_{defect} is the defect density.[9] This lifetime is inversely proportional to the defect density, thus under elevated defect concentrations, the neutral region SRH lifetime will shorten and may dominate device performance.

There are two important limits to consider for the diffusion-limited saturation current density, as described by Eq. (2) for the nBn. The first is the short absorber, or long diffusion length, limit, where $L_{diff} \gg L_{abs}$. For typical device architectures, high performance infrared detectors exhibit diffusion lengths far in excess of the absorber thickness. This limit may still apply in cases where defect concentrations are moderately elevated. If the limiting current mechanism is SRH generation in the neutral region, under the long diffusion length limit, Eq. (2) may be simplified and the reverse saturation current density for diffusion via this mechanism is described by

$$J_S^{SRH} = \frac{en_i^2 v\sigma L_{abs} N_{defect}}{N_{donor}}. \quad (4)$$

Notably, the dark current density is directly proportional to the defect density, and the thermal activation energy is equal to the full bandgap due to the temperature dependence of the n_i^2 factor.

Under higher defect concentrations, the diffusion length may reduce to a value much less than the absorber thickness. Here, the saturation diffusion current density is subjected to the long absorber, or short diffusion length, limit, where $L_{diff} \ll L_{abs}$. In this limit, Eq. (2) can again be simplified giving the defect-limited saturation current density as

$$J_S^{SRH} = \frac{en_i^2}{N_{donor}}\sqrt{D_p v\sigma N_{defect}}, \quad (5)$$

where D_p is the holes' diffusion coefficient. Here, the saturation current density is proportional to the square root of the defect density indicating a reduced dependence on defect concentration. If the nBn architecture is designed and fabricated so the absorber thickness is considerably longer than the diffusion length, even when diffusion length is long, this expression for the saturation current density will apply even under moderate defect concentrations.

The best nBn detectors to date operate in the long diffusion length limit and show current densities in excess of Rule 07, likely indicating moderate defect concentrations and performance limited by neutral region SRH generation, followed by minority carrier diffusion, as described by Eq. (3).[7] The predicted dark current as a function of defect concentration for an nBn detector natively in the long diffusion length limit is shown in Figure 1.

At low defect concentrations, the detector remains in the long diffusion length limit and shows a direct proportionality between dark current and defect concentration. At higher defect concentrations, the diffusion length reduces and the detector enters the short diffusion length regime where the current exhibits a reduced dependence on the density of defects. It is important to note that for nBn detectors with short absorber thicknesses, it is preferable to operate within the long diffusion length limit, even though this limit shows a greater dependence on defect density compared to the short diffusion length limit. The short diffusion length limit for these devices indicates significant damage to the epitaxial structure resulting in a noticeable reduction in the quantum efficiency.

The effects of two types of defects in nBn detectors are reported in the present study: defects due to lattice mismatch and due to exposure to proton irradiation. Detectors grown on mismatched substrates are subjected to dislocation defects. The defect concentration in the detector epitaxial structure depends on the thickness of the buffer layer between the substrate and the absorbing region, decreasing inversely with epitaxial layer thickness.[10] These effects were studied by examining InAs nBn and conventional photodiode detectors grown on matched and mismatched substrates. Temperature dependent current density-voltage (J-V) characteristics were measured and dark current density Arrhenius analysis was performed for lattice matched and lattice mismatched, nBn detectors (Figure 2). The lattice mismatched nBn detector was grown on a GaAs substrate.

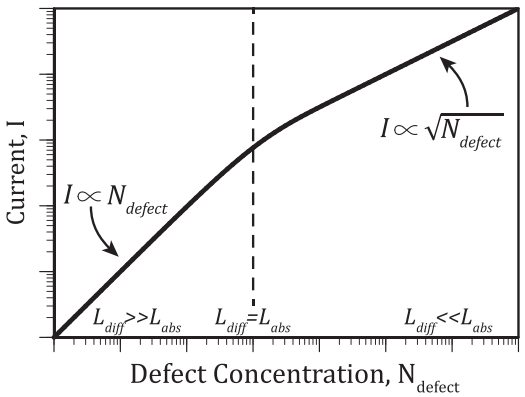

FIG. 1. Modeled nBn dark current as a function of increasing defect concentration for a detector natively in the long diffusion length limit. Under low defect concentrations, the detector remains in the long diffusion length limit, but under high defect concentrations, the detector enters the short diffusion length limit and the dark current dependence on the defect concentration reduces.

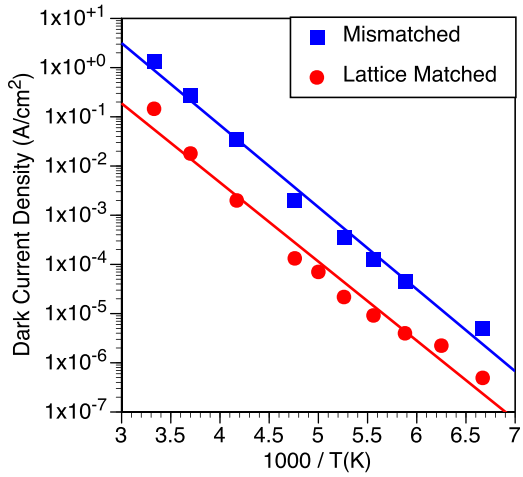

FIG. 2. Arrhenius analysis for dark current density of both lattice matched and mismatched InAs nBn detectors. Both detectors exhibit diffusion limited performance, as indicated by the slope of the lines that indicated full bandgap thermal activation energies; however, the mismatched substrate nBn shows dark currents elevated by an order of magnitude.

Both the lattice matched and mismatched InAs nBn detectors show diffusion limited performance with activation energies of 0.35 eV matching the bandgap of InAs, but the lattice mismatched nBn exhibits dark currents elevated by approximately an order of magnitude. The mismatched nBn has a significantly higher defect concentration and thus has elevated dark currents in accordance with SRH generation in the quasi-neutral region. It is important to note that SRH generation in the quasi-neutral region is a significantly smaller effect than SRH generation in a pn junction's depletion region.

Comparing the performance of InAs nBn detectors to conventional, InAs photodiodes demonstrate this effect as well as the difference in activation energies for the two related mechanisms (Figure 3).

The mismatched InAs nBn, indicated by the blue line in Figure 3, remains diffusion limited and maintains an activation energy of 0.35 eV or full bandgap activation, as described by Eq. (4), for the neutral-region SRH. The photodiode, shown in red, shows an elevated current density and an activation energy of 0.11 eV indicating a reduced thermal activation energy in accordance with depletion region SRH and Eq. (1). Under elevated defect levels, the nBn exhibits lower, but still elevated, defect densities and the full bandgap activation energy allows for more efficient reduction in the dark current with cooling compared to the defect limited photodiode.

A III-V semiconductor based, type-II strained-layer superlattice, MWIR, nBn has also been studied. This nBn has a Ga-free superlattice absorber with a 5.5 μm, 50% cutoff wavelength at 120 K and a typical nBn device architecture. The nBn was irradiated with 63MeV protons and current characteristics were measured at varying proton fluences. The dark current as a function of proton fluence is considered at a moderate bias of −300 mV (Figure 4).

It is assumed that increasing proton fluence scales directly with defect density. As expected, under very low proton fluences, the dark current exhibits very little change with increases in proton fluence. At low fluences, the device is primarily limited by defects native to the epitaxial structure. Once the defects induced by proton irradiation surpass the native defect concentration, the defects due to irradiation dominate. This device shows that the dark current is dependent on the square root of the proton fluence, or defect density, indicating this device is operating in the short diffusion length regime suggesting that the device was already severely defect limited by native defects even before irradiation.

The reverse bias J-V characteristics for both the lattice matched and mismatched InAs nBn and the irradiated MWIR nBn are shown in Figure 5.

For both the cases of defects induced via lattice mismatched growth and defects induced via proton irradiation, there is a clear increase in reverse saturation current density as predicted by the models and shown in Figures 2 and 4, respectively. It is of particular importance to note that for

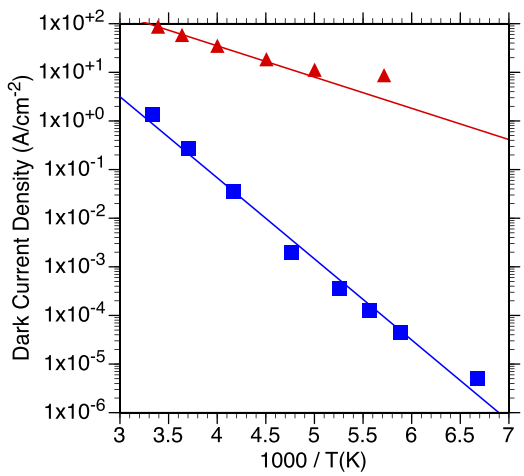

FIG. 3. Arrhenius analysis for an InAs nBn detector (blue) and a conventional photodiode (red) grown on GaAs substrates. Even under elevated defect concentrations, the nBn exhibits reduced dark current densities and full bandgap activation energies, whereas the photodiode exhibits a reduced activation energy.

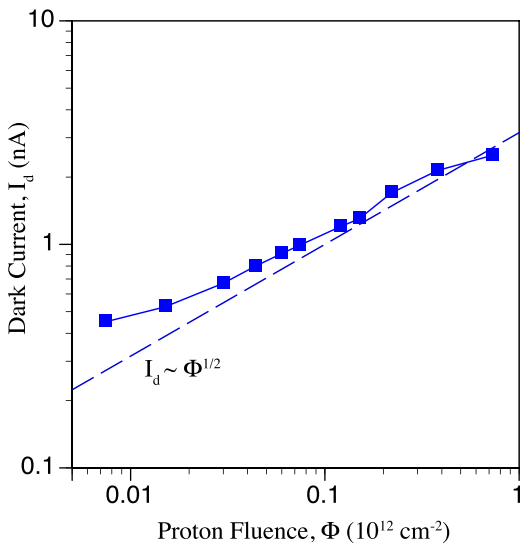

FIG. 4. Dark current as a function of proton fluence for an irradiated MWIR nBn detector. The detector exhibits a dark current dependence proportional to the square root of the defect density indicating SRH limited performance in the short diffusion length limit.

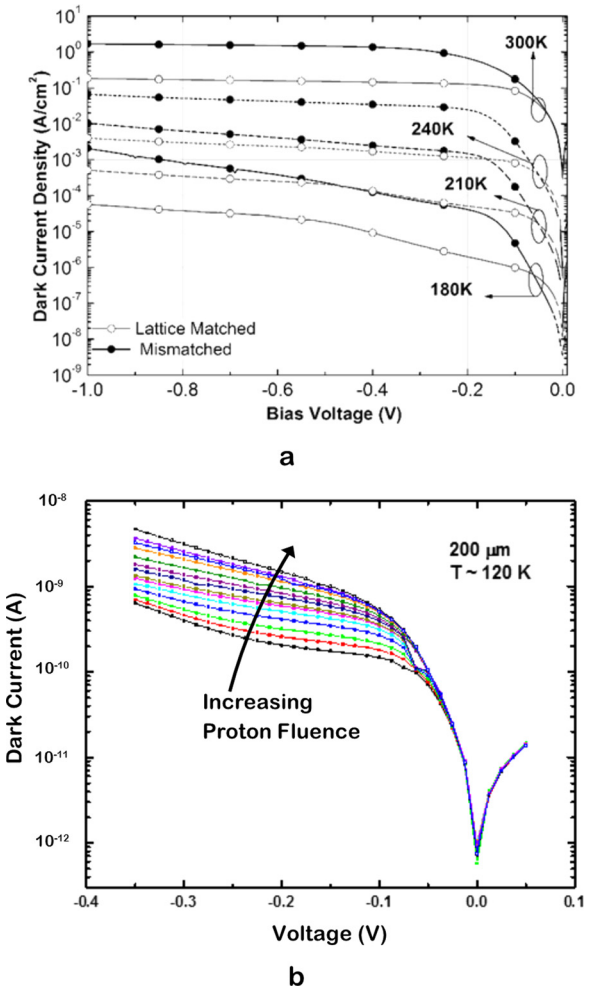

FIG. 5. Reverse bias J-V characteristics for the lattice matched and mismatched InAs (a) and the irradiated MWIR (b) nBn detectors. Both plots show that increasing the defect concentration increases the current at reverse biases greater than kT, but does not affect the reverse current at voltages near zero.

very low reverse biases, approximately less than −0.1 mV bias, neither of the induced defects resulted in change in the current characteristic around 0 V. This indicates that the defect-related diffusion current, which dominates at larger reverse biases, is not the dominant current mechanism at low reverse biases. Instead, low bias currents are apparently dominated by a mechanism that is unrelated to defects. Due to this, there is not a significant change in the zero-bias resistance with an increase in defect density for the nBn architecture; therefore, the zero-bias resistance area product, R_oA, is not a useful parameter to describe the performance of the nBn. This is contrary to the common use of R_oA as a figure of merit for conventional photodiodes because there is a correlation between the value of R_oA and the shot noise in photodiodes.[9]

In summary, nBn detectors with elevated defect concentrations show elevated dark currents but remain diffusion limited unlike defect-limited conventional pn junction based photodiodes which show significantly higher dark currents and a reduced activation energy indicating depletion region SRH limited performance. nBn detectors under moderate or high defect concentrations are limited by SRH generation in the quasi-neutral absorber, but are subjected to two different dependences on the defect density, depending on the diffusion length and the thickness of the absorbing region. It is important to note that for low native defect, nBn detectors with short absorber thicknesses, it is preferable to operate within the long diffusion length limit even though this limit shows a greater dependence on defect density compared to the short diffusion length limit. The short diffusion length limit indicates significant damage to the epitaxial structure resulting in a noticeable reduction in the quantum efficiency and increased noise.

This work was supported by the Army Research Office (W. Clark) and the Air Force Research Laboratory Space Vehicles Directorate.

[1]G. R. Savich, D. E. Sidor, X. Du, M. Jain, C. P. Morath, V. M. Cowen, J. K. Kim, J. F. Klem, D. Leonhardt, S. D. Hawkins, T. R. Fortune, A. Tauke-Pedretti, and G. W. Wicks, in *SPIE Defense + Security* (2014), pp. 907011–907016.
[2]V. M. Cowan, C. P. Morath, J. E. Hubbs, S. Myers, E. Plis, and S. Krishna, Appl. Phys. Lett. **101**(25), 251108 (2012).
[3]J. L. Johnson, L. A. Samoska, A. C. Gossard, J. L. Merz, M. D. Jack, G. R. Chapman, B. A. Baumgratz, K. Kosai, and S. M. Johnson, J. Appl. Phys. **80**, 1116–1127 (1996).
[4]W. Shockley and W. T. Read, Jr., Phys. Rev. **87**(5), 835 (1952).
[5]C.-T. Sah, R. N. Noyce, and W. Shockley, Proc. IRE **45**(9), 1228 (1957).
[6]W. E. Tennant, D. Lee, M. Zandian, E. Piquette, and M. Carmody, J. Electron. Mater. **37**(9), 1406 (2008).
[7]P. Martyniuk and A. Rogalski, Opt. Eng. **53**(10), 106105 (2014).
[8]P. G. Jespers, F. van de Wiele, and M. H. White, "Solid state imaging," in *Proceedings of the NATO Advanced Study Institute on Solid State Imaging, Louvain-la-Neuve, Belgium*, 3–12 September 1975 (Noordhoff, Leyden, 1976).
[9]A. Rogalski, K. Adamiec, and J. Rutkowski, *Narrow-Gap Semiconductor Photodiodes* (SPIE Press, Bellingham, 2000), 438 p.
[10]A. Krier and W. Suleiman, Appl. Phys. Lett. **89**(8), 083512 (2006).

Journal of ELECTRONIC MATERIALS, Vol. 45, No. 9, 2016
DOI: 10.1007/s11664-016-4451-3

Surface Leakage Mechanisms in III–V Infrared Barrier Detectors

D.E. SIDOR,[1,2] G.R. SAVICH,[1] and G.W. WICKS[1]

1.—The Institute of Optics, University of Rochester, Rochester, NY 14627, USA. 2.—e-mail: sidor@optics.rochester.edu

Infrared detector epitaxial structures employing unipolar barriers exhibit greatly reduced dark currents compared to simple pn-based structures. When correctly positioned within the structure, unipolar barriers are highly effective at blocking bulk dark current mechanisms. Unipolar barriers are also effective at suppressing surface leakage current in infrared detector structures employing absorbing layers that possess the same conductivity type in their bulk and at their surface. When an absorbing layer possesses opposite conductivity types in its bulk and at its surface, unipolar barriers are not solutions to surface leakage. This work reviews empirically determined surface band alignments of III–V semiconductor compounds and modeled surface band alignments of both gallium-free and gallium-containing type-II strained layer superlattice material systems. Surface band alignments are used to predict surface conductivity types in several detector structures, and the relationship between surface and bulk conductivity types in the absorbing layers of these structures is used as the basis for explaining observed surface leakage characteristics.

Key words: Unipolar barrier, infrared detector, superlattice, nBn, surface leakage

INTRODUCTION

Advanced photodetectors with epitaxial designs extending beyond simple pn junctions carefully manage the position of the Fermi level throughout the structure in order to suppress Shockley–Read–Hall (SRH) generation and associated generation–recombination (g–r) dark currents. In the most optimistic situation, junction-related SRH generation is greatly suppressed by ensuring that the Fermi level remains many k_BT away from the middle of the bandgap throughout the entire structure. The importance of this consideration increases exponentially as bandgap decreases: it is of primary importance in the small-bandgap absorbing layer of an infrared detector, where thermal generation through midgap states will readily proceed; but it becomes a less significant concern in large-bandgap layers, where the probability of half-bandgap thermal excitations is low.

Many examples of this type of advanced infrared photodetector exist. The introduction of the InAs(Sb) nBn in 2006 is an early example,[1] and it has since led to several variants of the more general unipolar barrier photodetector (UBP) device architecture.[2–5] The reported characteristics of these structures indicate that they are highly effective at suppressing bulk dark current mechanisms and are limited only by bulk diffusion current. The nBn and other UBP structures are also highly effective at suppressing surface leakage currents, *but only in some situations*. To date a high degree of success has been achieved in bulk designs employing InAs-like materials (e.g., InAs, InAsSb, and InGaAs), but similar results are not consistently achieved in type-II strained-layer superlattice (T2SL) detector designs. This work explores specific reasons why barrier architecture T2SL photodetectors may still be limited by surface leakage currents, and

(Received November 12, 2015; accepted March 5, 2016; published online March 23, 2016)

considers the general limitations of unipolar barriers for suppressing surface leakage.

BACKGROUND

InAs(Sb)-based bulk nBn detectors have demonstrated considerable improvements in dark current reduction over pn junction detectors formed in the same material.[6] At room temperature both structures are limited by bulk diffusion currents, but as the devices are cooled, diffusion current in the pn junction readily gives way to other mechanisms with little temperature dependence, whereas the nBn remains diffusion limited down to the noise floor of the measurement system. At this lower limit, the dark current in the nBn is reduced by a factor of approximately 10^6 compared to the pn junction, and it appears likely that a more sensitive measurement would resolve a continuation in this trend as further cooling is applied.

The nBn structure shown in Fig. 1 achieves diffusion-limited dark current performance in two important ways. First, junction-related SRH generation is avoided. The nBn contains no appreciable zero-bias depletion region; under normal operating conditions, an applied bias creates a small depletion region at the absorber-barrier interface; however, the Fermi level never approaches the middle of the bandgap in the absorbing layer, thereby eliminating associated g–r current. This is an obvious distinction between the nBn and pn junction. Second and somewhat less obviously, the large-bandgap barrier layer, which blocks the flow of majority carrier electrons in the bulk, also blocks the flow of the majority of carrier electrons along the *n*-type surface of the device, thus the nBn exhibits no surface leakage current (see Fig. 2). Indeed, for this reason it is an essential feature of the InAs(Sb) nBn design that each material layer within the structure employs a bulk conductivity type that matches its surface conductivity type.

In spite of the successful suppression of surface leakage by unipolar barriers in bulk detector designs, this success is not always duplicated in superlattice-based detectors. Consequently, many researchers are actively investigating surface leakage current and surface passivation in T2SL infrared detectors. For example, Knorr et al. at the U.S. Army Research Laboratory[7] and Plis et al. at the University of New Mexico[8] are investigating various chemical passivation strategies for both InAs and GaSb surfaces; Chen et al. at Northwestern University[9] are producing gated diodes that bias mesa sidewalls; and Aifer et al. at the Naval Research Laboratory[10] are utilizing epitaxial "W" structures in which large-bandgap layers isolate the small-bandgap infrared absorbing layer. The diversity of present research efforts by these and other groups provides a clear indication that unipolar barriers do not enjoy the same success at blocking surface leakage currents when applied to superlattice detector designs.

SURFACE CONDUCTIVITY OF III–V COMPOUNDS

In order to understand why unipolar barriers may be effective in blocking surface currents as implemented in bulk structures but not in superlattices, consider the relative band alignments of various III–V compounds. Previously, empirical observations reported by several authors led to the realization that the difference in Schottky barrier heights formed between two different semiconductor materials joined to metal contacts also corresponded to the conduction band discontinuity (for an *n*-type Schottky barrier) or valence band discontinuity (for a *p*-type Schottky barrier) between the two materials.[11–13] Figure 3 is a graphical depiction of the band alignment data published by Tiwari and Frank,[12] and makes use of the fact that the surface Fermi level, derived from measurements of Schottky barrier heights, exists at the same absolute energy for various materials. In the present work, it is emphasized that this same empirical model can

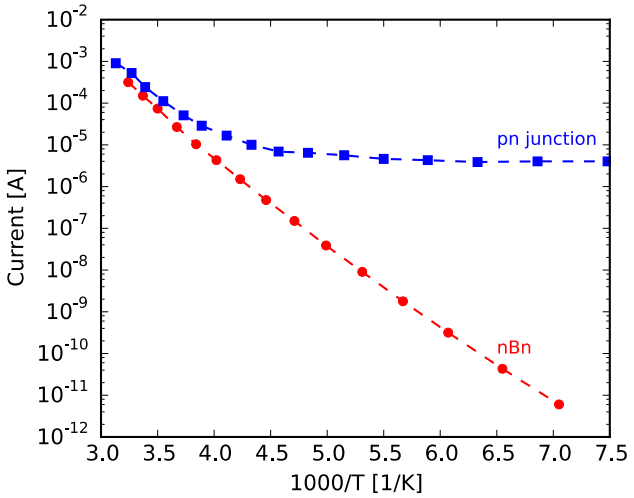

Fig. 1. Arrhenius plot of dark currents in an InAs nBn (red circles) and pn junction (blue squares) (Color figure online).[6]

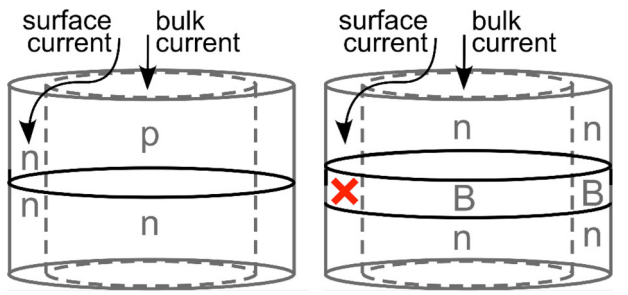

Fig. 2. Left: InAs pn junction with *n*-type surface leakage pathway. Right: InAs nBn with large-bandgap barrier layer that blocks surface leakage current.

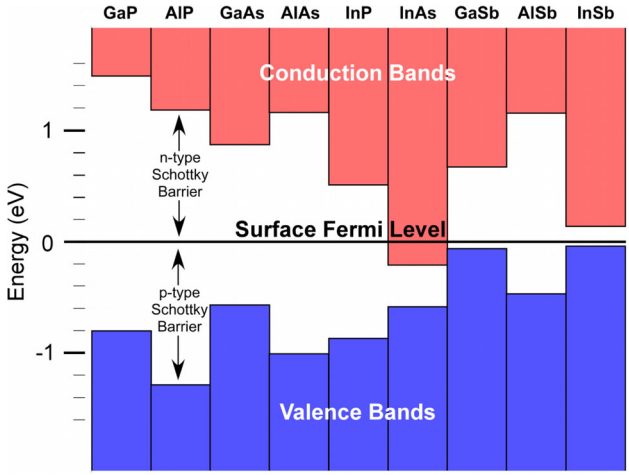

Fig. 3. Conduction and valence band energies relative to the surface Fermi level for various III–V semiconductor materials.[12,14]

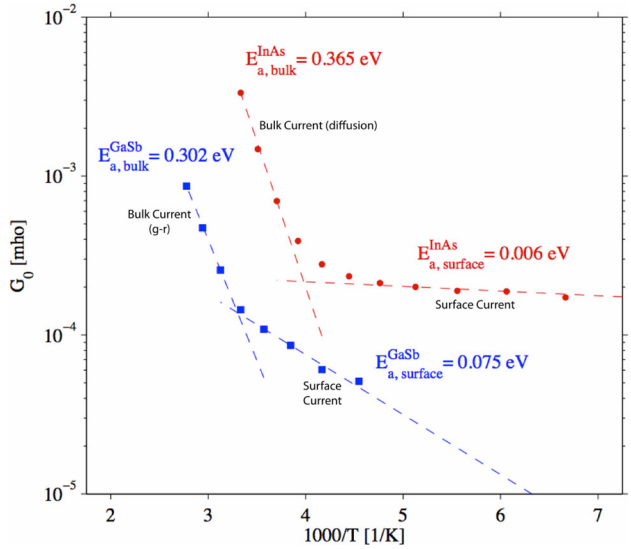

Fig. 4. Arrhenius analysis of conductance of InAs (red circles) and GaSb (blue squares) pn junctions, showing transition from bulk-limited to surface-limited performance (Color figure online).

be used to determine the surface conductivity type of a given material by comparing the surface Fermi level position to the locations of the conduction and valence band edges. From a historical perspective, the ability to precisely control bulk conductivity type through the use of impurity doping distinguished semiconductors as a unique class of materials, and thus it seems consideration is often given only to bulk conductivities when creating epitaxial designs. However, the practical implications of surface Fermi level pinning in III–V infrared detector materials require that careful consideration also be given to surface conductivity type, and to the relation between surface and bulk conductivities.

The present empirical model implies that most III–V compounds have surface Fermi levels located inside the bandgap, which creates depleted surfaces, but there are significant exceptions. InAs and InAs-rich ternaries have degenerate *n*-type surfaces, with the surface Fermi level in InAs being pinned approximately 100 meV above the conduction band minimum. GaSb has a non-degenerate *p*-type surface, with the surface Fermi level pinned approximately 70–90 meV above the valence band minimum. This model, therefore, predicts the surfaces of these two compounds to be highly conductive, and that the density of charge carriers at the surface should be only weakly temperature-dependent (GaSb) or temperature-independent (InAs).

In accordance with this prediction, surface conductivity in both InAs and GaSb has been experimentally measured.[14] The pn homojunctions were grown in each material and processed into mesa devices using contact photolithography and wet chemical etching. The InAs pn junction consisted of 2.3 μm of *n*-type material ($n = 1 \times 10^{16}$), followed by 0.5 μm of *p*-type material ($p = 1 \times 10^{18}$), and a 1000 Å p^+ contact layer ($p = 1 \times 10^{19}$), grown on an InAs substrate. The GaSb pn junction consisted of 1.0 μm of *n*-type material ($n = 5 \times 10^{17}$), followed by 0.3 μm of *p*-type material ($p = 5 \times 10^{17}$), and a 150 Å p^+ contact layer ($p = 1 \times 10^{19}$), grown on a GaSb substrate. No attempts were made to passivate the surface of either sample.

Arrhenius analysis of device conductance was performed, and results for 210 μm × 210 μm square mesas are shown in Fig. 4. At or above room temperature both materials exhibit strongly temperature-dependent and readily identifiable current characteristics. The conductance of the InAs pn junction shows a thermal activation of 365 meV, approximately equal to the full bandgap and indicative of diffusion current; the conductance of the GaSb pn junction shows a thermal activation energy of 302 meV, approximately equal to one half of the full bandgap and indicative of SRH generation in the depletion region followed by drift. In this temperature range the performance of both devices is dominated by bulk mechanisms.

A different type of behavior is seen in both materials as the devices are cooled. The conductance of the InAs pn junction becomes nearly temperature-independent below approximately 200 K, whereas the conductance of the GaSb pn junction transitions to a thermal activation energy of 75 meV below approximately 300 K. This is consistent with the above picture: the degenerate surface of InAs is populated with carriers at all temperatures, whereas the non-degenerate surface of GaSb exhibits a thermal activation energy given by the separation between the valence band edge and surface Fermi level, typically reported to be in the range of 70–90 meV. In this temperature range the performance of both devices is dominated by surface mechanisms. Because bulk dark currents are strong exponential functions of temperature, but surface currents are weakly temperature-

dependent (GaSb) or temperature-independent (InAs), unmitigated surface leakage quickly becomes a limiting factor as devices employing these materials are cooled.

EXTENSION TO SUPERLATTICES

Recent results allow for similar deductions to be made about superlattice materials. Modeling by Flatté and Grien[15] indicates that so-called "Ga-free" InAs/InAsSb superlattices will have band edge locations relative to the universal surface Fermi level that will produce degenerate *n*-type surfaces. Similarly, the band edge locations of "Ga-containing" InAs/GaSb superlattices are likely to possess non-degenerate *n*-type surfaces. Modeled band offsets relative to InAs and GaSb allow for these materials to be visualized alongside the materials of Fig. 3. Figure 5 summarizes the band alignments of these superlattice materials and their binary constituents.

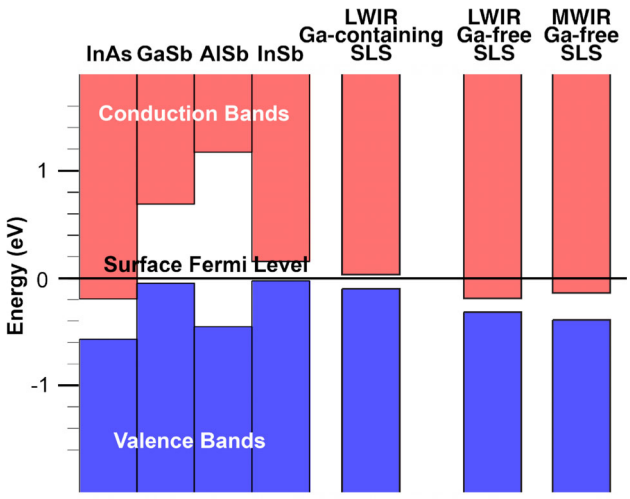

Fig. 5. Extension of the Schottky barrier model of surface band alignments to include T2SL infrared detector materials.[12,15]

The observation that both the Ga-free and Ga-containing material systems for mid-wave infrared (MWIR) and long wavelength infrared (LWIR) superlattices are likely to possess *n*-type surfaces is significant, because current-generation T2SL photodetectors sometimes employ p-doped absorbing regions. This is for a good reason, as photogenerated minority carrier electrons are more readily able than holes to tunnel from layer to layer through the structure. However, it creates the undesirable situation in which the bulk and surface conductivity types in the absorbing region differ from one another. Consider such a device structure that incorporates a unipolar barrier to block the flow of bulk majority carrier holes. If minority carrier electrons are allowed to flow in the bulk, as must be the case for the detector to operate, then majority carrier electrons cannot be blocked at the surface, and significant surface leakage current is the expected result (Fig. 6).

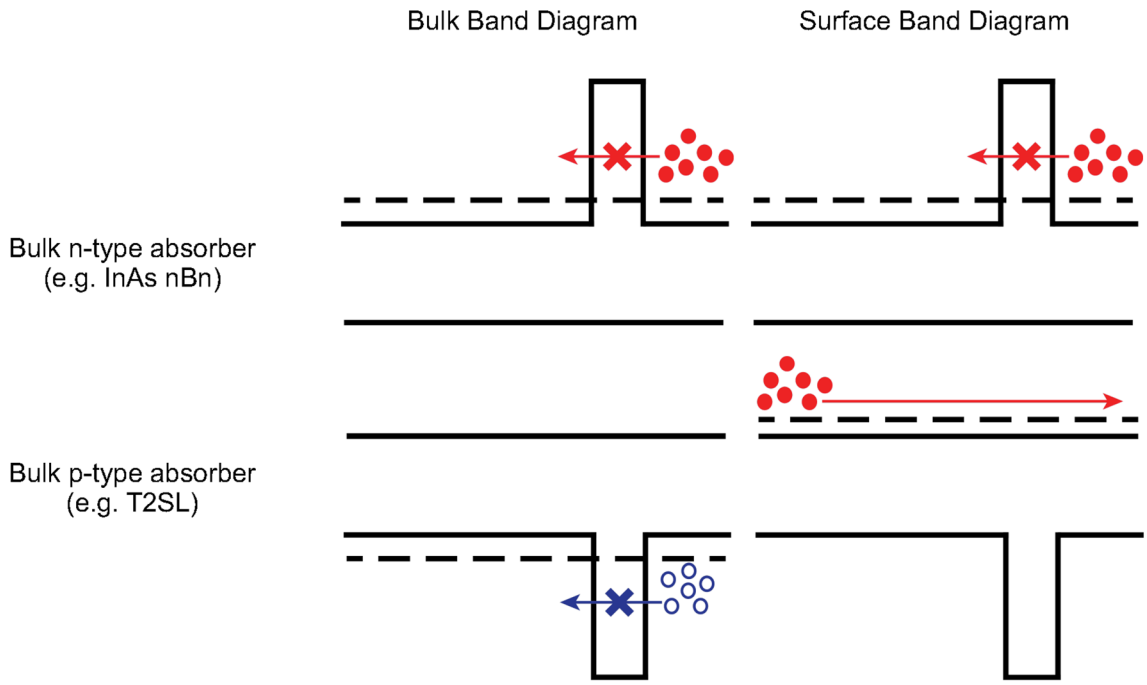

Fig. 6. Top row: A unipolar barrier detector incorporating an *n*-type absorber material with an *n*-type surface blocks bulk majority carriers (electrons) and surface leakage current (electrons). Bottom row: A unipolar barrier detector incorporating a *p*-type absorber material with an *n*-type surface blocks bulk majority carriers (holes) but cannot block surface leakage current (electrons).

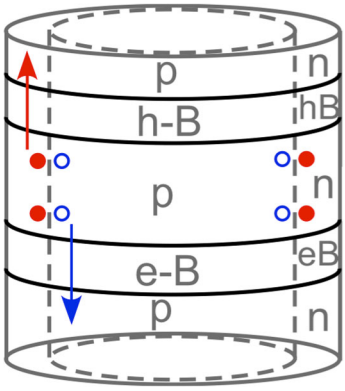

Fig. 7. Complementary barrier structure incorporating p-doped absorber layer with *n*-type surface. A pn junction exists in the subsurface region of the absorber layer, and resulting g–r current cannot be blocked by an electron barrier or a hole barrier.

COMMENT ON COMPLEMENTARY BARRIER STRUCTURES

We have argued that simple unipolar barrier detectors cannot suppress surface leakage current when the absorbing layer is doped to have the opposite conductivity type of its surface. However, if this situation cannot be avoided, some benefit can be derived by employing a more complex epitaxial structure containing both electron and hole barriers, somewhat similar to the complementary barrier infrared detector (CBIRD) architecture developed by Ting et al.[4] Complementary barrier structures include two large-bandgap blocking layers, one extending into the conduction band and the other into the valence band. One barrier can block the bulk majority carriers; the other barrier can block the surface majority carriers. The barriers are positioned on opposite ends of the structure, such that neither electrons nor holes can flow unimpeded through the entire structure, but photocurrent can still be extracted because photogenerated electrons can flow over the hole barrier while photogenerated holes can flow under the electron barrier.

Complementary barrier designs are effective at blocking surface currents that are carried by a single carrier type across the entire structure. However in any material layer that is doped to have a bulk conductivity type opposite to that of its surface, a pn junction must form in the transition region between bulk and surface (refer to the device structure shown in Fig. 7). The depletion region of this pn junction creates the opportunity for subsurface SRH generation and associated g–r current. If this occurs in the absorbing layer of a photodetector, then the g–r current cannot be blocked by a unipolar barrier, because it shares the same spatial makeup as the photocurrent.[16] Therefore, under the condition that the absorbing layer of a detector must be doped to have the opposite conductivity type of its surface, unipolar barriers represent at best a partial solution to the problem of surface leakage current.

CONCLUSIONS

In summary, the well-established empirical connection between Schottky barrier heights and energy band discontinuities provides a means to assess the surface conductivities of semiconductor materials. This model agrees with experimental measurements of degenerate *n*-type InAs and nondegenerate *p*-type GaSb surfaces. The model suggests that Ga-free, and likely also Ga-containing superlattice infrared materials should possess *n*-type surfaces. Unipolar barriers have been shown to effectively suppress surface leakage current in photodetectors with absorbing regions that have the same conductivity type in their bulk and at their surface. When the absorbing layer is doped to have a bulk conductivity type opposite to that of its surface, complementary unipolar barriers may be able to reduce surface leakage, but may be unable to suppress it completely.

ACKNOWLEDGEMENTS

This work was supported by the U.S. Army Research Office and by the Air Force Research Laboratory Space Vehicles Directorate, Kirtland AFB.

REFERENCES

1. S. Maimon and G.W. Wicks, *Appl. Phys. Lett.* 89, 15 (2006).
2. P. Klipstein, O. Klin, S. Grossman, N. Snapi, I. Lukomsky, D. Aronov, M. Yassen, A. Glozman, T. Fishman, and E. Berkowicz, *Opt. Eng.* 50, 6 (2011).
3. B.-M. Nguyen, S. Bogdanov, S. Abdollahi Pour, and M. Razeghi, *Appl. Phys. Lett.* 95, 18 (2009).
4. D.Z.-Y. Ting, A. Soibel, C.J. Hill, J. Nguyen, S.A. Keo, B. Rafol, B. Yang, M.C. Lee, J.M. Mumolo, and J.K. Liu, *Infrared Phys. Technol.* 54, 3 (2011).
5. G.W. Wicks, G.R. Savich, J.R. Pedrazzani, and S. Maimon, *Proc. SPIE* 7608, 760822 (2010).
6. J.R. Pedrazzani, S. Maimon, and G.W. Wicks, *Electron. Lett.* 44, 25 (2008).
7. D.B. Knorr Jr., K.S. Williams, N.F. Baril, C. Weiland, J.W. Andzelm, J.L. Lenhart, J.C. Woicik, D.A. Fischer, M.Z. Tidrow, and S.V. Bandara, *Appl. Surf. Sci.* 320, 414 (2014).
8. E.A. Plis, M. Narayanan-Kutty, and S. Krishna, *Laser Photon. Rev.* 7, 1 (2013).
9. G. Chen, E.K. Huang, A.M. Hoang, S. Bogdanov, S.R. Darvish, and M. Razeghi, *Appl. Phys. Lett.* 101, 21 (2012).
10. E.H. Aifer, J.H. Warner, C.L. Canedy, I. Vurgaftman, E.M. Jackson, J.G. Tischler, J.R. Meyer, S.P. Powell, K. Olver, and W.E. Tennant, *J. Electron. Mater.* 39, 7 (2010).
11. F.L. Schuermeyer, P. Cook, E. Martinez, and J. Tantillo, *Appl. Phys. Lett.* 55, 18 (1989).
12. S. Tiwari and D.J. Frank, *Appl. Phys. Lett.* 60, 5 (1992).
13. A.D. Katnani and G. Margaritondo, *Phys. Rev. B* 28, 4 (1983).
14. D.E. Sidor, G.R. Savich, and G.W. Wicks, *Proc. SPIE* **9616**, 96160U-1 (2015).
15. M.E. Flatté and C.H. Grein, *Proc. SPIE* **9370**, 93700K-1 (2015).
16. G.R. Savich, J.R. Pedrazzani, D.E. Sidor, S. Maimon, and G.W. Wicks, *Appl. Phys. Lett.* 99, 12 (2011).

Appendix F

Surface Conduction in InAs and GaSb

D. E. Sidor*[a], G. R. Savich[a], G. W. Wicks[a]
[a]The Institute of Optics, University of Rochester, Rochester NY, 14627

ABSTRACT

This work presents a fundamental investigation of the surface conduction pathways occurring along etched sidewalls in devices fabricated from InAs and GaSb. Surface leakage currents are identified by their dependence on device size and thermal activation energy, and are characterized in terms of sheet conductance. InAs is found to have a temperature-independent sheet conductance of approximately 8×10^{-8} mho×square. The sheet conductance of GaSb is comparable to that of InAs at room temperature, and when cooled it decreases with a thermal activation energy of 75 meV, which is approximately equal to the known separation between the valence band and surface Fermi level. The temperature dependence of the surface conductance of the two materials indicates that the surface of InAs is degenerate and the surface of GaSb is non-degenerate.

Keywords: InAs, GaSb, Surface conductivity, Photodetector, Superlattice, Unipolar barrier

1. INTRODUCTION

III-V semiconductor materials belonging to the 6.1Å family (InAs, GaSb, AlSb, and their alloys and superlattices) are increasingly used to produce high performance MWIR and LWIR photodetectors. Barrier architecture detectors fabricated from these materials exhibit competitively low dark current densities compared to state-of-the-art pn-based structures. Appropriately placed unipolar barriers within these structures serve to block dark currents arising from growth- and/or processing-related defects, and from radiation-induced defects, such as those occurring in space-bound systems. Unipolar barrier structures can also be designed to effectively block surface leakage currents, providing the mechanism of surface conduction is understood, which is investigated in this study.

A significant challenge inherent to working with these materials is presented by their conducting surfaces: regardless of bulk doping level, InAs possesses a degenerate n-type surface and GaSb possesses a nondegenerate p-type surface. Care must therefore be taken to avoid fabricating structures in which surface conduction pathways unintentionally shunt the intended bulk conduction. The detrimental effects of conducting surfaces become more significant as device size is reduced, thereby making surface electrical characteristics a particularly important consideration for applications where detector package size and weight are constrained.

2. BACKGROUND

It has been known for decades that, in general, the location of the Fermi level relative to the valence and conduction band edges at the exposed surfaces of a semiconductor material differs from the Fermi level location deep inside bulk material[1]. Exposed surfaces are locations where the crystal lattice of the semiconductor terminates and dangling bonds result, for example at the final growth surface, and on vertical sidewalls revealed by etching. The specific location of the Fermi level at an exposed surface depends on the identity of the material in question; but for a given material, the surface Fermi level is fixed to a particular location independent of bulk material properties. A summary of early results pertaining to a wide variety of materials has been compiled by Tiwari and Frank[2]. Figure 1 is a graphical representation derived from their work.

Initial investigations of surface band alignments were conducted in the context of measuring Schottky barrier heights formed between semiconductors and metal contacts. Questions were asked whether the observed pinning of the surface Fermi level was an intrinsic property of the semiconductor surface, or perhaps an extrinsic property of the semiconductor/metal interface or of defects introduced during sample preparation. It was observed that Schottky barrier heights were independent of the work function of the contact metal used, implying that the pinning effect was due to the population of additional electronic states at the semiconductor surface[1]. Subsequent investigations of clean surfaces revealed some cases where surface Fermi level pinning occurred and other cases where it did not; but either way, exposing clean surfaces to small amounts of metal, oxygen, and hydrogen all resulted in surface Fermi level pinning[3].

Nanophotonics and Macrophotonics for Space Environments IX, edited by Edward W. Taylor,
David A. Cardimona, Proc. of SPIE Vol. 9616, 96160U · © 2015 SPIE
CCC code: 0277-786X/15/$18 · doi: 10.1117/12.2188878

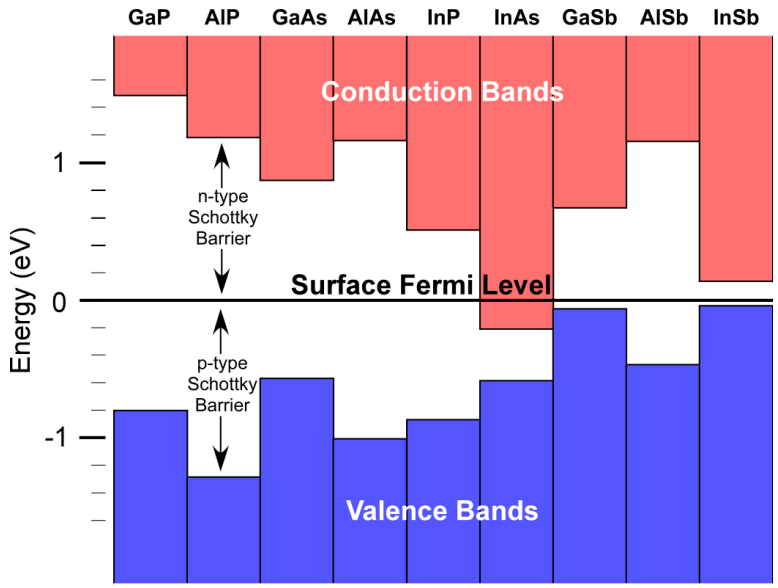

Figure 1. Surface Fermi level pinning in a variety of III-phosphides, -arsenides and –antimonides[2].

These various observations led to the generally accepted conclusion that surface Fermi level pinning is caused by large densities of defect states that result from impurity adsorption. Semiconductor material processed into device structures is necessarily exposed all of these impurities. Therefore, while Fermi level pinning may not be a fundamental property of all pristine semiconductor surfaces, it is nonetheless an unavoidable property of the surfaces of practical devices created with modern process technologies.

Many of the III-phosphide, -arsenide and -antimonide materials depicted in Figure 1 have surface Fermi levels pinned in the bandgap. The surfaces of these materials are depleted of charge carriers and thus are highly resistive. Practical effects of depleted surfaces have been reported in GaAs, for example, in several different contexts. One example is a reduction in the apparent thickness of doped layers for Hall measurements;[4] another is a drastic reduction in nanowire conductivity below a certain critical feature dimension[5].

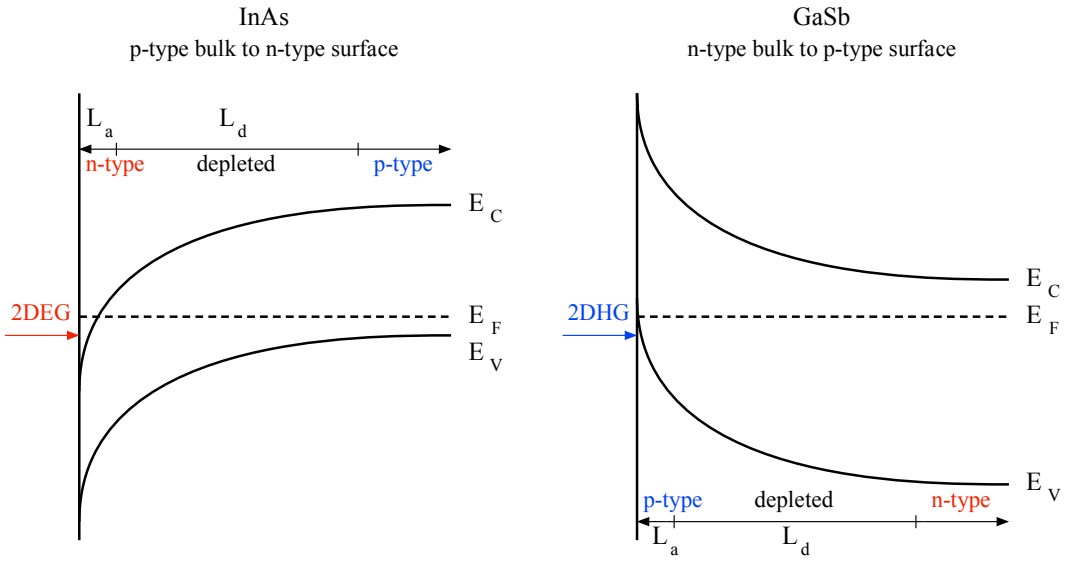

Figure 2. Band alignments at the accumulated surfaces of p-type bulk InAs and n-type bulk GaSb. The bulk conducting regions are surrounded by depletion layers of thickness L_d and surface accumulation layers of thickness L_a. Two dimensional electron gases (2DEG) and hole gases (2DHG) exist at the surfaces of InAs and GaSb, respectively.

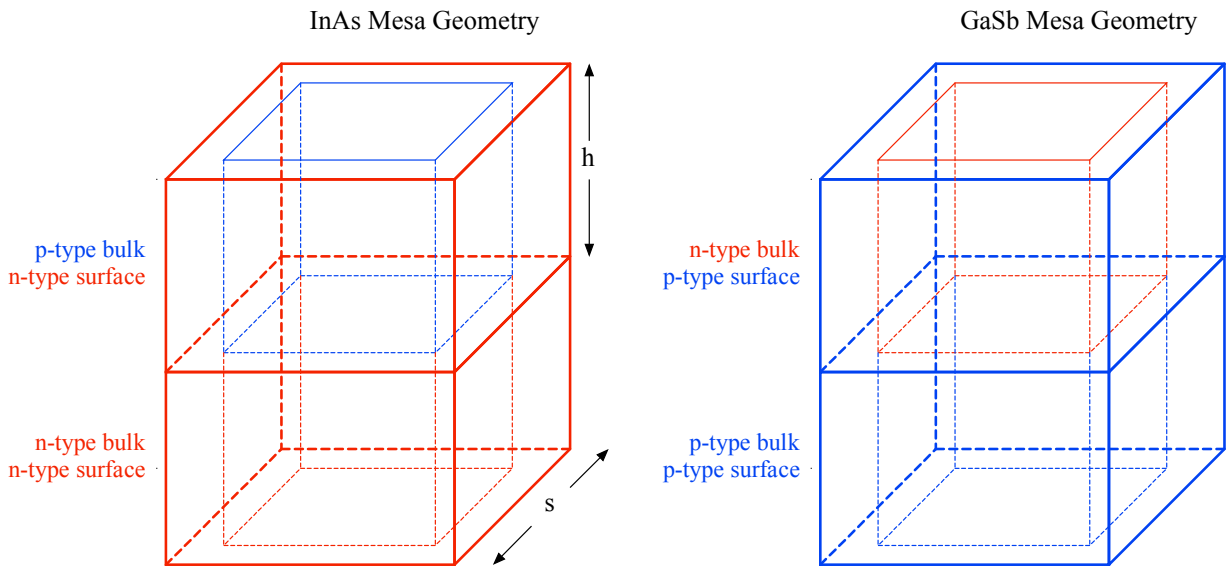

Figure 3. Geometry of conducting regions in InAs and GaSb pn junction mesa structures. Surface Fermi level pinning causes the p-type InAs layer to have an n-type surface, and the n-type GaSb layer to have a p-type surface.

Note however that Figure 1 also contains several smaller-bandgap materials whose surface Fermi levels are not pinned within the gap, but are pinned near (or in) an energy band. Significant examples of this type of behavior include InAs and GaSb, two materials that are currently drawing a great deal of interest for use in infrared detector structures. These materials have accumulated surfaces rather than depleted surfaces: in the case of InAs, the surface Fermi level is pinned inside the conduction band, resulting in a degenerate n-type surface. The surface Fermi level is pinned near the valence band in GaSb, resulting in a nondegenerate p-type surface (see Figure 2).

Both depleted and accumulated surfaces can result in unwanted device characteristics. Whereas depleted surfaces manifest in a reduction of the cross-sectional area of the electrically active conducting region of a device, accumulated surfaces present a potentially more insidious problem. When an accumulated surface traverses the full length of a device, and the conductivity type at the surface differs from the conductivity type in the bulk, a second and unintended conduction pathway through the device is created. This unintended surface conduction pathway serves to shunt the intended bulk conduction pathway, resulting in significant surface leakage current. This effect has been frequently observed, and has been the motivating factor in many studies of passivation techniques and other mitigation strategies such as the insertion of unipolar barriers.[6] Parallel surface and bulk conduction pathways are shown as an equivalent circuit diagram in Figure 4.

Bulk current in a pn junction under reverse bias usually exhibits a strong exponential dependence on temperature. Sufficiently high-quality material is limited by diffusion current created by Auger generation, which proceeds with a thermal activation energy approximately equal to the full bandgap of the material. Defect states present in the junction lead to Shockley-Read-Hall generation, which is characterized by reverse current exhibiting a thermal activation energy approximately equal to half of the bandgap of the material. These two bulk mechanisms are dominant at higher operating temperatures, but because of their strong dependence on temperature, they are effectively reduced by device cooling. In contrast, surface current varies more slowly with temperature. The nondegenerate surface of GaSb is populated with carriers that are excited from the surface Fermi level into the valence band, across an energy difference of approximately 70 meV[1]. The degenerate surface of InAs is populated with charge carriers at all temperatures because the surface Fermi level is located inside the conduction band. As shown in Figure 5, once a device has been cooled to the point that surface leakage has become the dominant reverse bias dark current mechanism, further cooling is no longer an effective method for reducing the dark current.

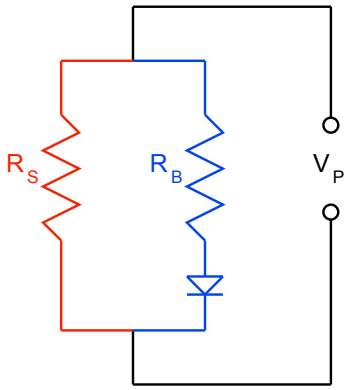

Figure 4. Equivalent circuit diagram showing the intended bulk diode pathway and unintended surface resistor pathway that exist in parallel in a pn junction structure grown in a material with an accumulated surface.

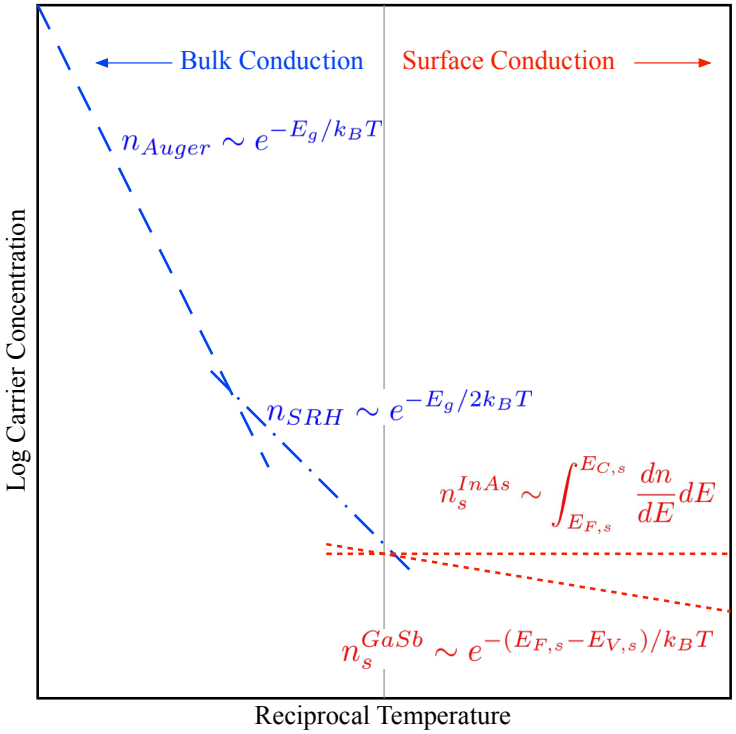

Figure 5. Thermal characteristics of bulk and surface current generation mechanisms in a pn junction structure consisting of a material with an accumulated surface. Bulk diode currents under reverse bias exhibit strong temperature dependences. Surface current in GaSb is weakly temperature dependent, and surface current in InAs is temperature independent.

3. EXPERIMENT

InAs and GaSb pn junctions were grown by molecular beam epitaxy (MBE) in a Riber 32P solid source MBE reactor. These materials were then processed into square mesa structures using contact photolithography, phosphoric,

sulfuric, and hydrochloric acid-based etchants, and thermal evaporation of gold contacts. Mesa side lengths ranged from s=30 to 210 microns. Samples were electrically contacted in a Lakeshore cryogenic probe station configured for dark current measurements. Dark current-voltage (IV) characteristics were measured at various temperatures ranging from 360K to 100K.

4. ANALYSIS

The zero-bias differential conductance G_0 is defined as the slope of the tangent line to an IV curve at zero voltage,

$$G_0 = \left.\frac{dI}{dV}\right|_{V=0} \tag{1}$$

Note that G_0 is the reciprocal of the zero-bias differential resistance R_0, a familiar and important figure of merit in the analysis of photodiodes. The zero-bias differential conductance consists of contributions from both the surface and bulk conduction pathways shown schematically in Figure 3 and in the equivalent circuit diagram of Figure 4. The surface and bulk conduction pathways are connected in parallel, so the total conductance of a device is the sum of surface and bulk contributions

$$G_0 = G_{0,S} + G_{0,B} \tag{2}$$

The experimentally measured conductance of a device depends on material properties and device geometry, both of which vary between the surface and bulk conduction pathways. The surface and bulk contributions are given by

$$G_{0,S} = \frac{4(sL_a - L_a^2)}{h}\sigma_s \tag{3}$$

$$G_{0,B} = \frac{(s - 2L_a - 2L_d)^2}{h}\sigma_B \tag{4}$$

where σ_S and σ_B are surface and bulk conductivities, respectively, s is the square mesa side length, L_a is the surface accumulation length (the thickness of the two-dimensional electron or hole gas that forms when the surface and bulk conductivity types differ), and L_d is the depletion length between the surface and bulk conducting regions. If $s \gg L_a$ and $s \gg L_d$, as are the case for the range of mesa sizes investigated here, then to a good approximation $G_{0,S} \propto s$ and $G_{0,B} \propto s^2$.

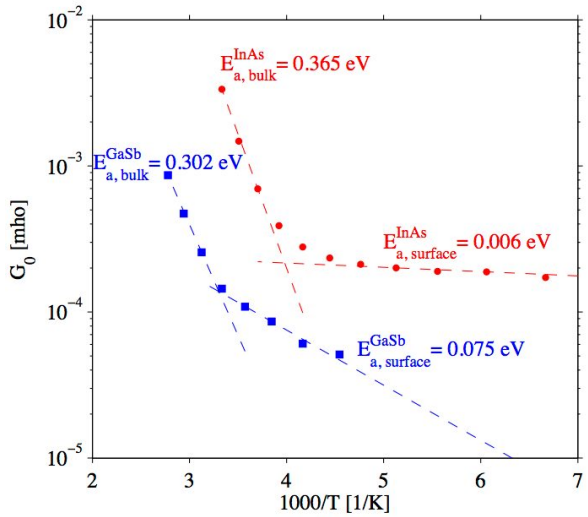

Figure 6. Arrhenius plots of conductance for 210μm square InAs and GaSb pn junction devices.

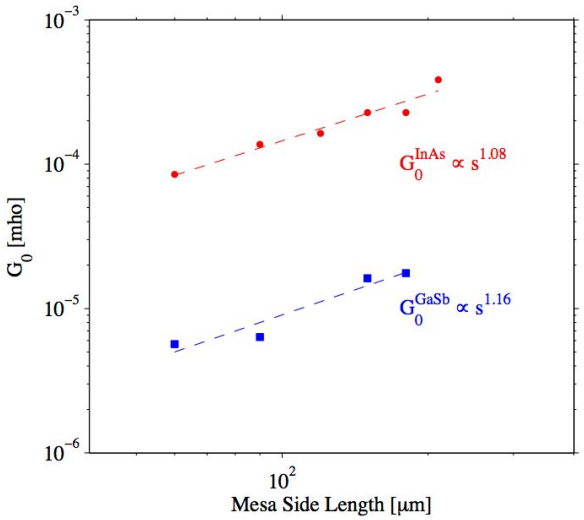

Figure 7. Size dependence of conductance for InAs and GaSb pn junction devices measured at 200K.

Close to room temperature, both materials exhibit bulk-limited conductance. The conductance of the InAs device decreases with a thermal activation energy approximately equal to the InAs bandgap, indicating that the dominant

current mechanism is Auger generation followed by minority carrier diffusion. The conductance of the GaSb device decreases with a thermal activation energy approximately equal to one half of the GaSb bandgap, indicating SRH generation and associated generation-recombination current.

At temperatures below about 200K the bulk currents in both materials decrease sufficiently so that surface current becomes the limiting dark current mechanism. This can be seen in two ways. First, the thermal activation energy of the dark current at these lower temperatures behaves as expected according to the surface band alignments. The InAs device shows a nearly temperature-independent conductance, consistent with its degenerate surface. The surface of GaSb is nondegenerate, and as such, the conductance of the GaSb device continues to slowly decrease with a thermal activation energy equal to the separation between the surface Fermi level and valence band, about 75 meV. Additional evidence that the low-temperature conductance is dominated by the surface, is provided by examining its size dependence. Surface currents are expected to scale in proportion to the mesa side length s, whereas bulk currents scale as s^2. At 200K and below, the conductance of the InAs devices varies with mesa side length to the power 1.08, and the conductance of the GaSb devices varies with mesa side length to the power 1.16, confirming their identification as surface-dominated currents.

Thin film terminology is used to express the final result in a geometry-independent manner. Sheet conductance is defined as the conductance of a surface multiplied by the number of "squares" measured along the direction of current flow, and is given by

$$\widetilde{G_S} = G_S \times \frac{h}{4s} \tag{5}$$

where the ratio h/s is the aspect ratio of a mesa sidewall. The experimentally determined sheet conductances for the InAs and GaSb pn junctions investigated in this work is given in Table 1.

Table 1. Summary of results.

Material	Surface Type	Surface E_a [meV]	$\widetilde{G_S}$ [mho×□] (200K)
GaSb	p-type	75	2×10^{-8}
InAs	n-type	6	8×10^{-8}

5. CONCLUSION

Surface currents in InAs and GaSb pn junctions have been identified by their size and temperature dependence, and the conducting surfaces of these materials have been characterized in terms of sheet conductance. Arrhenius analysis clearly shows that InAs has a degenerate surface. The surface Fermi level is pinned inside the conduction band, and the resulting electron population at the surface is essentially unaffected by cooling the device. The behavior of GaSb pn junctions is consistent with the nondegenerate surface of that material, where the surface Fermi level is pinned approximately 75 meV from the valence band. This small energy separation causes the surface current in GaSb to be weakly temperature-dependent. Surface leakage currents arise in devices fabricated from these materials when they incorporate layers of differing surface and bulk conductivity types.

REFERENCES

[1] Mead, C. A. and Spitzer, W. G., "Fermi Level Position at Semiconductor Surfaces," Phys. Rev. Lett. 10(11), 471-472 (1963).

[2] Tiwari, S. and Frank, D. J., "Empirical fit to band discontinuities and barrier heights in III-V alloy systems," Appl. Phys. Lett. 60(5), 630-632 (1992).

[3] Spicer, W. E., Chye, P. W., Skeath, P. R., Su, C. Y., and Lindau, I., "New and unified model for Schottky barrier and III-V insulator interface states formation," J. Vac. Sci. & Technol. 16(5), 1422-1433 (1979).

[4] Chandra, A., Wood, C. E. C., Woodward, D. W., and Eastman, L. F., "Surface and interface depletion corrections to free carrier-density determinations by Hall measurements," Solid-State Electronics 22, 645-650 (1979).
[5] Gutsche, C., Lysov, A., Regolin, I., Münstermann, B., Prost, W., and Tegude, F. J., "Scalable Electrical Properties of Axial GaAs Nanowire pn-Diodes," J. Elec. Mater. 41(5), 809-812 (2011).
[6] Maimon, S. And Wicks, G. W., "nBn detector, an infrared detector with reduced dark current and higher operating temperature," Appl. Phys. Lett. 89(15), 151109 (2006).

DISTRIBUTION LIST

DTIC/OCP
8725 John J. Kingman Rd, Suite 0944
Ft Belvoir, VA 22060-6218 1 cy

AFRL/RVIL
Kirtland AFB, NM 87117-5776 2 cys

Official Record Copy
AFRL/RVSW/David Cardimona 1 cy

(This page intentionally left blank)